Molecular electronic excitations calculated from a solid-state approach: Methodology and numerics

P. H. Hahn,[1] W. G. Schmidt,[2] and F. Bechstedt[1]
[1]*Institut für Festkörpertheorie und -optik, Friedrich-Schiller-Universität, Max-Wien-Platz 1, 07743 Jena, Germany*
[2]*Theoretische Physik, Universität Paderborn, 33098 Paderborn, Germany*
(Received 13 September 2005; revised manuscript received 31 October 2005; published 30 December 2005)

We investigate the applicability and accuracy of a solid-state approach, which was developed originally for the relatively homogeneous electron gas, to describe electronic single-particle and electron-hole pair excitations in molecules. Thereby we start from the determination of the molecular ground state within the local density functional theory using repeated supercells and pseudopotentials for the electron-ion interaction. The electronic spectra are obtained from the Green's function formalism. The exchange-correlation self-energy Σ is linearly expanded in the screened Coulomb interaction, i.e., the GW approximation is used. Optical spectra are obtained from the Bethe-Salpeter equation for the irreducible polarization propagator. The numerical implementation and possible pitfalls of this methodology are discussed using silane, disilane, and water molecules as examples. In particular the influence of the dynamics of the screening, the supercell size, and the number of empty states are studied. The resulting single- and two-particle excitation energies are compared with experiment and previous theoretical work.

DOI: 10.1103/PhysRevB.72.245425 PACS number(s): 71.15.Qe, 31.15.Lc, 31.25.−v, 33.20.−t

I. INTRODUCTION

Organic functionalization of solid substrates has become a rapidly evolving research branch involving both chemistry and physics. Moreover, in many instances systems of biological relevance are studied, such as proteins or nucleic acids adsorbed on solid surfaces. The interest in these systems is fueled by applications such as chemical or biological sensors[1] or molecule-based electronic circuits.[2] It has stimulated a large number of experimental and theoretical studies, see, e.g., Refs. 3 and 4.

In order to explain and predict spectroscopic, electronic, chemical, and photochemical properties of hybrid systems composed of both molecules and solid surfaces, their ground- and excited-state properties need to be computed. The ground-state properties of a wide class of systems, including atomic and molecular aggregates, clusters, as well as crystalline solids can be efficiently calculated from *first principles* using the density functional theory (DFT)[5,6] in either the local density approximation (LDA)[6–8] or by using an improved exchange-correlation (XC) functional, e.g., the generalized gradient approximation (GGA)[9,10] or hybrid functionals.[11,12] This scheme generally yields very good results for atomic structures and binding energies at reasonable computational costs, as demonstrated by a very large number of computational studies in the last two decades. However, the use of the DFT-LDA/GGA as a theoretical tool for the study of physical properties other than the ground state, as in the calculation of electronic spectra (e.g., photoemission, inverse photoemission, electron-energy loss) or optical spectra (e.g., luminescence, absorption, reflectance anisotropy), is *a priori* not justified: The Kohn-Sham eigenvalues of the effective, noninteracting single particles of the DFT can neither be interpreted as electron removal or addition energies nor as energies of neutral electronic excitations, such as electron-hole pairs. This problem can be overcome in part by working in the "delta self-consistent field" (ΔSCF) scheme. It has been used for the calculation of ionization potentials, electron affinities, or quasiparticle gaps[13,14] as well as for electron-hole pair energies.[15]

There is a variety of quantum-chemical methods to compute electronic excitations for isolated atoms and molecules, for a recent review see, e.g., Ref. 16. Among them are *ab initio* single-configurational methods that use the Hartree-Fock (HF) solution as reference wave function, e.g., the so-called configuration interaction-singles (CIS) method.[17] It overestimates the excitation energies due to the absence of correlation effects and the multiconfigurational character of the states. The size-extensive coupled-cluster (CC) approach in different versions[18,19] is also often used for excited-state calculations. In general, a HF zeroth-order reference is used. Excited-state calculations carried out using the time-dependent density functional theory (TDDFT)[20–22] are becoming more and more popular because of their simplicity and apparent black-box behavior. By solving a frequency-dependent polarizability equation for the excitation energy and the transition dipole moment, it avoids the explicit calculation of the excited states. TDDFT approaches seem to have no rival when computing excited states in large molecules, e.g., C_{70},[23] from *first principles*.

A completely different type of method to calculate excited-state properties is referred to as propagator[24,25] or Green's function approaches.[26–28] The latter were originally developed to describe the many-body interactions in a rather homogeneous electron gas such as formed in crystalline solids. They start from the screening response of the electronic system after electronic or optical excitation. Accordingly, the dynamically screened or shielded Coulomb interaction W instead of the bare Coulomb potential v is the central quantity used in these methods. The excitation energies correspond to the poles of single- and two-particle Green's functions[26,27,29,30] that are obtained by means of a many-body

 ©2005 The American Physical Society

perturbation theory. By evaluating the one-electron Green's function G, single-particle excitations, e.g., ionization energies and electron affinities, are derived that can be measured in photoemission and inverse photoemission spectroscopies. Two-particle Green's functions of the electronic system, e.g., the irreducible polarization propagator P or the density-density response function L, allow one to access electron-hole pair energies and collective excitations, e.g., plasmons, which may be observed in optical spectroscopies or electron-energy loss spectroscopy (EELS).

Due to numerical limitations, the exact calculation of the correlation energy in solids is hardly possible. Instead, one resorts to approximations to describe the most relevant correlation mechanisms. Hedin's so-called GW approach,[26,27] which represents a linear expansion of the XC self-energy operator Σ of the electrons in the screened potential W instead of the bare Coulomb potential v (which gives only the exchange interaction), is the most widely used approximation in this context. This scheme allows for deriving a single-quasiparticle (QP) equation of a structure similar to the Kohn-Sham equation used in the DFT.[31,32] Only the (semi-)local potential V^{XC} is replaced by the XC self-energy operator Σ. This suggests to calculate QP bands by using a first-order perturbative approach with respect to $(\Sigma - V^{XC})$.[33–35] However, QP transition energies do in general not correctly describe optical excitation energies, i.e., photon absorption processes. The interaction of electron-hole pairs may dramatically shift the peak positions as well as appreciably distort the spectral line shape. The electron-hole interaction is accounted for by solving the Bethe-Salpeter equation (BSE) for the irreducible polarization function P.[36,37] Starting from DFT-LDA/GGA calculations, it has recently become possible to solve the BSE from *first principles*. Optical spectra including the effects of electron-hole interaction were obtained for a series of bulk semiconductors and insulators[38–42] and their surfaces.[43,44] The formalism has been generalized also for the calculation of nonlinear optical spectra.[45,46]

The methodological developments concerning the calculation of molecular excitations on one hand, and of excitations in extended solids on the other hand, have advanced rather independently of each other for a long time. However, the progress in materials science has recently caused intense interest in phenomena that involve excitations of systems like organically functionalized semiconductors[47] or small clusters embedded in a solid matrix.[48] Thus a sufficiently accurate approach that is applicable to longitudinal electron-electron interactions in systems with both highly localized and extended electronic states is required to assist in the design of such systems. The most accurate quantum-chemistry methods such as configurational interaction (CI) schemes[18,19] are computationally very demanding and can hardly be applied to large systems such as crystals and their surfaces. Presently, there are many activities aimed at applying TDDFT to extended systems.[49–51] However, the accuracy of excitation energies obtained within TDDFT for systems that extend beyond the exciton radius is not yet established. On the other hand, there is no fundamental reason why Green's function techniques based on the perturbative GW approach should be restricted to solids. In fact, there are already a number of promising attempts to apply these methods to atoms, molecules, or small clusters, see, e.g., Refs. 52–59. The present paper aims at exploring systematically the potential and possible pitfalls of applying a GW/BSE implementation based on a Bloch function description of the electronic states (as typically used for crystalline solids) to small molecules. Particular attention is paid to a detailed description of the methodological and numerical details.

We study three prototypical molecules, monosilane (SiH_4), disilane (Si_2H_6), and water (H_2O). These molecules are studied using a three-step approach: (i) Ground-state calculations are performed within the DFT-LDA or DFT-GGA. The Kohn-Sham eigenvalues and eigenfunctions are obtained for the theoretical equilibrium geometry. (ii) Then we solve the quasiparticle equation in a perturbative manner with respect to $(\Sigma - V^{XC})$. The influence of the usually neglected nondiagonal elements of the self-energy $\Sigma = GW$ and the energy dependence of Σ are studied. We will show that an expansion of the self-energy matrix elements around the KS eigenvalues is inappropriate for molecules because of the huge QP shifts. (iii) Molecular optical spectra that account for electron-hole attraction and electron-hole exchange are obtained by solving the BSE.

The paper is organized as follows: A brief summary of the theoretical and computational methods is given in Sec. II. Methodological and numerical details of the implementation are investigated in Sec. III using SiH_4 as an example. In Sec. IV single- and two-particle excitation energies are presented for Si_2H_6 and H_2O. The paper closes with a brief summary and conclusions in Sec. V.

II. THEORETICAL AND COMPUTATIONAL METHODS

A. Ground state

The structurally relaxed electronic ground states of the considered molecules were determined by DFT total-energy calculations.[5,6] The convergence criterion for the Hellmann-Feynman forces was set to 1 meV/Å. For silane and disilane, the LDA functional in the Perdew-Zunger parameterization[7,8] was used to model the XC effects. The electron-ion interaction is described by *first-principles* norm-conserving pseudopotentials that have been generated within the Hamann scheme.[60] A real-space finite-difference representation of the electronic wave functions, densities, and potentials together with a multigrid technique allow for convergence acceleration and efficient parallelization of the calculations.[61] The wave functions were mapped on grids with a spacing of about 0.25 Å. In order to make contact with earlier work on excitations in ice,[42] the GGA[9,10] is used to describe exchange and correlation for H_2O molecules. In this case, the mesh point spacing has been reduced to 0.16 Å and soft Troullier-Martins pseudopotentials[62] were used.

To model the molecules in the gas phase we used a periodic arrangement of *sc* supercells, each containing one molecule. The supercell must be large enough to avoid interactions between the molecule and its images. The convergence of the bound electronic excitations within 0.1 eV with varying the supercell size was the criterion used to determine the necessary cell dimension. This led to edge lengths of $a_s = 11.9$ Å (SiH_4), 13.8 Å (Si_2H_6), and 10.0 Å (H_2O). For si-

lane we also present results for supercell dimensions up to 35.5 Å. The translational symmetry of the supercell arrangement leads to Bloch wave vectors in the corresponding Brillouin zone (BZ). However, since the dispersion of the resulting KS bands is vanishing for noninteracting molecules, we sample the BZ with one point only, that was placed just beside the Γ point.

In order to check the influence of the numerical implementation, the properties of silane were also calculated using the projector-augmented wave (PAW) method[63] in conjunction with a plane-wave representation of the wave functions. Thereby we used the DFT-LDA implementation of the Vienna Ab-initio Simulation Package (VASP).[64] The all-electron-like wave functions of the PAW scheme allow for a highly accurate evaluation of matrix elements of the Coulomb interaction[48] as well as of the optical transition operator.[65] The results obtained using VASP agree within 0.01 Å for the structural properties and 0.1 eV for the excitation energies with the findings obtained from the real-space multigrid code.

Irrespective of the representation of the wave functions, for a given atomic geometry the Kohn-Sham equation[6]

$$\left[-\frac{\hbar^2}{2m}\Delta_{\mathbf{x}} + V_{ion}(\mathbf{x}) + V_H(\mathbf{x})\right]\psi_\lambda(\mathbf{x}) + V^{XC}(\mathbf{x})\psi_\lambda(\mathbf{x}) = \varepsilon_\lambda\psi_\lambda(\mathbf{x}) \tag{1}$$

has to be solved self-consistently for the external potential $V_{ion}(\mathbf{x})$ due to the ions by iterating the Hartree potential $V_H(\mathbf{x})$, the XC potential $V^{XC}(\mathbf{x})$, and the electron density

$$n(\mathbf{x}) = \sum_{\lambda=1}^{N} |\psi_\lambda(\mathbf{x})|^2. \tag{2}$$

The sum in Eq. (2) runs over all occupied states of the N-electron system. Each KS state is characterized by an eigenfunction $\psi_\lambda(\mathbf{x})$, an eigenenergy ε_λ, and a set of single-particle quantum numbers λ. For a periodic supercell arrangement, λ may be replaced by a band index ν and Bloch wave vector $\mathbf{k}$.

The Lagrangian parameters ε_λ in the KS equation (1) do not represent energies of single-particle excitations. Apart from the energy of the highest occupied state that equals the ionization energy,[32] they have no physical meaning. Nevertheless, the KS eigenvalues are used in many instances as a first approximation to the true single-particle excitation energies. This is motivated by the similarity of Eq. (1) with the single-particle Schrödinger equation. For bulk crystals, the band dispersions obtained from the KS equation are indeed similar to those of measured Bloch bands.[33–35] Irrespective of their interpretation, the solutions $\{\psi_\lambda(\mathbf{x})\}$ of Eq. (1) form an orthonormal and complete set of functions well-suited to represent the Green's functions of interest.

B. Quasiparticle equation

Single-particle excitations are measured in photoemission and inverse photoemission experiments. There are two obvious reasons why the excitation energies obtained in these experiments usually deviate from the corresponding KS eigenvalues: (i) The excited electron or defect electron, i.e., hole, is not independent of its surroundings. The electronic system reacts to the excitation by redistributing the electrons, i.e., by screening. The excited electron or hole is dressed and forms a quasiparticle.[66] This dressing changes the energy required to remove or add an electron to the system. (ii) The excitation of the system changes the number of electrons, N. The KS eigenvalues are, however, calculated for the system in the ground state with N electrons. To overcome this limitation, the propagation of an electron or hole is described by the single-particle Green's function whose poles in the frequency plane define the excitation energies. Using a variational procedure, Hedin[26,27] derived a self-contained set of five coupled equations. The equation of motion of the single-particle Green's function has a structure similar to the Kohn-Sham equation (1)

$$\left[i\hbar\frac{\partial}{\partial t} + \frac{\hbar^2}{2m}\Delta_{\mathbf{x}} - V_{ion}(\mathbf{x}) - V_H(\mathbf{x})\right]G(11') - \int \Sigma(12)G(21')d2 = \delta(1-1') \tag{3}$$

with $1=\mathbf{x}t$ and $1'=\mathbf{x}'t'$. The most notable difference is the replacement of the exchange-correlation potential V^{XC} by the XC self-energy Σ. The Green's function and the self-energy have to be determined self-consistently through a set of coupled equations,

$$\Sigma(12) = i\hbar\int W(1^+3)G(14)\Gamma(42;3)d(34), \tag{4}$$

$$W(12) = v(12) + \int W(13)P(34)v(42)d(34), \tag{5}$$

$$P(12) = -i\hbar\int G(23)G(42)\Gamma(34;1)d(34), \tag{6}$$

$$\Gamma(12;3) = \delta(12)\delta(13) + \int \frac{\delta\Sigma(12)}{\delta G(45)}G(46)G(75)\Gamma(67;3)d(4567), \tag{7}$$

where W is the screened Coulomb potential, P the polarization function, and Γ the vertex function. In addition

$$\varepsilon(12) = \delta(12) - \int v(13)P(32)d3 \tag{8}$$

yields the dielectric function which determines the screening

$$W(12) = \int v(13)\varepsilon^{-1}(32)d3 \tag{9}$$

of the longitudinal electron-electron interaction in the system due to the bare Coulomb potential $v(11')=e^2/|\mathbf{x}-\mathbf{x}'|\,\delta(t-t')$. Starting with the Hartree approximation, where $\Sigma=0$, the vertex and polarization functions result as

$$\Gamma(12;3) = \delta(12)\delta(13), \tag{10}$$

$$P_0(12) = -i\hbar\, G(12)G(21). \tag{11}$$

This leads to the GW approximation of the self-energy

$$\Sigma(12) = i\hbar\, G(12)W(1^+2). \tag{12}$$

The dielectric function (8) occurring in the screened Coulomb interaction (9) of expression (12) has to be calculated within the random-phase approximation (RPA) (11) or, more precisely, the independent-quasiparticle approximation.

In general, no Lehmann representation of the single-particle Green's function exists.[27,56] The single-particle wave functions and eigenvalues depend on the energy. Usually, the spectral function possesses more than one peak.[67,68] Satellite structures appear, reducing the spectral strength of the main peak. If the latter is very pronounced, it is a reasonable approximation to neglect the satellites and to assign the full spectral strength to this so-called quasiparticle peak. The lifetime of the quasiparticle determines the width of the QP peak. In the following we assume an infinite lifetime by neglecting the width of the QP peak. In thermodynamic equilibrium at temperature T, the Green's function for imaginary time differences $t-t'$ can be expressed in terms of QP wave functions $\psi_\lambda^{\mathrm{QP}}(\mathbf{x})$ and energies $\varepsilon_\lambda^{\mathrm{QP}}$ by

$$G(\mathbf{x}\mathbf{x}', t-t') = \frac{1}{-i\hbar\,\beta}\sum_n e^{-iz_n(t-t')}\sum_\lambda \frac{\psi_\lambda^{\mathrm{QP}}(\mathbf{x})\psi_\lambda^{\mathrm{QP}*}(\mathbf{x}')}{\hbar z_n - \varepsilon_\lambda^{\mathrm{QP}}} \tag{13}$$

with $\beta = 1/k_B T$ and $\hbar z_n = \mu - in\pi/\beta$ ($n = \pm 1, \pm 3, \pm 5, \ldots$; μ is the chemical potential of electrons). In this Lehmann representation, we have implicitly assumed that QP wave functions and energies are independent of the energy $\hbar z_n$. This is true only for quasiparticles with a sharply peaked spectral function and often approximately the case for states of nonmetallic systems around the band gap.[67,68] We will later show that this holds also for quasiparticles in molecules. The representation (13) of the Green's function leads to the eigenvalue problem for the quasiparticles

$$\left[-\frac{\hbar^2}{2m}\Delta_{\mathbf{x}} + V_{ion}(\mathbf{x}) + V_H(\mathbf{x})\right]\psi_\mu^{\mathrm{QP}}(\mathbf{x}) + \int d^3\mathbf{x}'\,\Sigma(\mathbf{x}\mathbf{x}', \varepsilon_\mu^{\mathrm{QP}})\psi_\mu^{\mathrm{QP}}(\mathbf{x}') = \varepsilon_\mu^{\mathrm{QP}}\psi_\mu^{\mathrm{QP}}(\mathbf{x}). \tag{14}$$

The equation of motion for both the Kohn-Sham and quasiparticle wave function are quite similar. This suggests to expand the QP wave functions in terms of Kohn-Sham orbitals according to

$$\psi_\mu^{\mathrm{QP}}(\mathbf{x}) = \sum_\lambda A_{\mu\lambda}\psi_\lambda(\mathbf{x}). \tag{15}$$

Using this expansion in the quasiparticle equation, one obtains an eigenvalue problem for the expansion coefficients and the quasiparticle energies in the form

$$\sum_{\lambda'}(\delta_{\lambda\lambda'}\varepsilon_\lambda + \mathrm{Re}\langle\lambda|\Sigma(\varepsilon_\mu^{\mathrm{QP}}) - V^{XC}|\lambda'\rangle)A_{\mu\lambda'} = \varepsilon_\mu^{\mathrm{QP}}A_{\mu\lambda}, \tag{16}$$

where the matrix element is explicitly given by

$$\langle\lambda'|\Sigma - V^{XC}|\lambda\rangle = \int d^3\mathbf{x}\int d^3\mathbf{x}'\,\psi_{\lambda'}^*(\mathbf{x})\{\Sigma(\mathbf{x}\mathbf{x}', \varepsilon_\mu^{\mathrm{QP}}) - V^{XC}(\mathbf{x})\delta(\mathbf{x}-\mathbf{x}')\}\psi_\lambda(\mathbf{x}'). \tag{17}$$

If the nondiagonal elements of the operator $\delta\Sigma(\varepsilon) = \Sigma(\varepsilon) - V^{XC}$ are negligible, one gets the first-order perturbation theory result. The quasiparticle wave functions are replaced by the Kohn-Sham wave functions $\psi_\lambda^{\mathrm{QP}}(\mathbf{x}) = \psi_\lambda(\mathbf{x})$,[31] and the quasiparticle energies are given by

$$\varepsilon_\lambda^{\mathrm{QP}} = \varepsilon_\lambda + \Delta_\lambda,$$

$$\Delta_\lambda = \mathrm{Re}\langle\lambda|\Sigma(\varepsilon_\lambda^{\mathrm{QP}}) - V^{XC}|\lambda\rangle. \tag{18}$$

It is clear from this expression that the influence of the precise functional used to describe V^{XC} in the DFT calculations on the quasiparticle energies can be expected to be minor. In most actual implementations, the self-energy difference in Eq. (18) is not taken at the QP energy $\varepsilon_\lambda^{\mathrm{QP}}$, but expanded linearly around the KS eigenvalue ε_λ. Furthermore, the Green's function in G and W in the GW expression (12) are replaced by the KS Green's function G_0, leading to the so-called G_0W_0 approximation. The QP shifts (18), $|\Delta_\lambda| = |\varepsilon_\lambda^{\mathrm{QP}} - \varepsilon_\lambda|$, are rather large for molecules, however. Therefore the linear expansion is not a good approximation. Instead, we follow the Blomberg-Bergersen approach[69,70] and replace the Green's function in Σ [Eq. (12)] and W [Eq. (5)] by a Green's function of the form(13) with the KS orbitals as QP wave functions.

C. Exchange-correlation self-energy

The calculation of the matrix elements of the exchange-correlation potential V^{XC} is straightforward. Somewhat more complicated to evaluate, however, are the matrix elements of the self-energy operator Σ. With the screened Coulomb potential in a Bloch-Fourier representation and a symmetrized inverse dielectric function

$$W_{\mu\mu'\mathbf{k}'}^{\nu\nu'\mathbf{k}}(\tilde{z}_m) = \frac{4\pi e^2}{\Omega}\sum_{\mathbf{q},\mathbf{G},\mathbf{G}'}\frac{B_{\nu\nu'}^{\mathbf{k}\mathbf{k}'}(\mathbf{q}+\mathbf{G})B_{\mu\mu'}^{\mathbf{k}\mathbf{k}'*}(\mathbf{q}+\mathbf{G}')}{|\mathbf{q}+\mathbf{G}||\mathbf{q}+\mathbf{G}'|}\varepsilon^{-1}(\mathbf{q}+\mathbf{G}, \mathbf{q}+\mathbf{G}'; \tilde{z}_m) \tag{19}$$

one obtains the matrix element (17) of the self-energy in GW approximation as

$$\langle\nu\mathbf{k}|\Sigma(\hbar z_n)|\mu\mathbf{k}\rangle = -\frac{1}{\beta}\sum_{n'}\sum_{\mathbf{k}'}\sum_{\nu'}W_{\mu\nu'\mathbf{k}'}^{\nu\nu'\mathbf{k}}(z_n - z_{n'})G_{\nu'\nu'}(\mathbf{k}', z_{n'}). \tag{20}$$

Here $B_{\nu\nu'}^{\mathbf{k}\mathbf{k}'}(\mathbf{Q})$ denotes the Fourier transform of two Bloch functions

$$B^{\mathbf{k}\mathbf{k}'}_{\nu\nu'}(\mathbf{Q}) = \int d^3\mathbf{x}\,\psi^*_{\nu\mathbf{k}}(\mathbf{x})e^{i\mathbf{Q}\mathbf{x}}\psi_{\nu'\mathbf{k}'}(\mathbf{x}). \tag{21}$$

The diagonal matrix elements of the Green's function are given by

$$G_{\nu\nu}(\mathbf{k},z) = \frac{1}{\hbar z - \varepsilon^{\mathrm{QP}}_{\nu}(\mathbf{k})}. \tag{22}$$

The wave vector $\mathbf{q}$ in Eq. (19) samples the BZ, and the wave vectors $\mathbf{G}$ and $\mathbf{G}'$ are reciprocal lattice vectors. With the polarization function in the GW approximation, $P=-i\hbar GG$, the symmetrized dielectric function in Eq. (19) follows in independent-quasiparticle approximation as

$$\varepsilon(\mathbf{q}+\mathbf{G},\mathbf{q}+\mathbf{G}';\omega) = \delta_{\mathbf{G}\mathbf{G}'} + \frac{8\pi e^2}{\Omega|\mathbf{q}+\mathbf{G}||\mathbf{q}+\mathbf{G}'|} \sum_{cv,\mathbf{k}\mathbf{k}'} \left[\frac{B^{\mathbf{k}\mathbf{k}'}_{cv}(\mathbf{q}+\mathbf{G})B^{\mathbf{k}'\mathbf{k}}_{vc}(\mathbf{q}+\mathbf{G}')}{\varepsilon^{\mathrm{QP}}_{c}(\mathbf{k}) - \varepsilon^{\mathrm{QP}}_{v}(\mathbf{k}') + \hbar(\omega+i\eta)} + \frac{B^{\mathbf{k}'\mathbf{k}}_{vc}(\mathbf{q}+\mathbf{G})B^{\mathbf{k}\mathbf{k}'}_{cv}(\mathbf{q}+\mathbf{G}')}{\varepsilon^{\mathrm{QP}}_{c}(\mathbf{k}) - \varepsilon^{\mathrm{QP}}_{v}(\mathbf{k}') - \hbar(\omega+i\eta)} \right], \tag{23}$$

where the c sum (v sum) is over empty (filled) states. The required self-consistency of the QP energies $\varepsilon^{\mathrm{QP}}_{\nu}(\mathbf{k})$ in the Green's function (22) and the dielectric matrix (23) complicates the computation of the matrix elements (20). It renders the computations time demanding, despite the neglect of the difference between QP and KS wave functions in the self-energy Σ itself. The starting point usually employed for calculations of extended systems, the replacement of $\varepsilon^{\mathrm{QP}}_{\lambda}$ by ε_{λ}, is not well-suited for molecules, where the quasiparticle energies are much closer to the Hartree-Fock (HF) values than to the Kohn-Sham energies. In explicit computations, assuming unchanged wave functions, we replace the quasiparticle energies $\varepsilon^{\mathrm{QP}}_{\lambda}$ by HF-like values $\varepsilon^{\mathrm{HF}}_{\lambda}$ for starting the iterations. These HF-like eigenvalues are determined from the unscreened exchange contribution to the GW self-energy Σ, which is, however, computed using the KS wave functions (see discussion below).

The spectral representation of the symmetrized inverse dielectric function

$$\varepsilon^{-1}(\mathbf{q}+\mathbf{G},\mathbf{q}+\mathbf{G}';\tilde{z}) = \delta_{\mathbf{G}\mathbf{G}'} + \int_{-\infty}^{+\infty} \frac{d\omega}{\pi} \frac{\mathrm{Im}[\varepsilon^{-1}(\mathbf{q}+\mathbf{G},\mathbf{q}+\mathbf{G}';\omega)]}{\tilde{z}-\omega} \tag{24}$$

allows for splitting the self-energy, $\Sigma=\Sigma^X+\Sigma^C$, into an energy-independent exchange term and a correlation part which is frequency dependent. For zero temperature it holds

$$\Sigma^X_{\nu\mu}(\mathbf{k}) = -\frac{4\pi e^2}{\Omega}\sum_{\nu',\mathbf{k}'}^{occ}\sum_{\mathbf{q},\mathbf{G}} \frac{B^{\mathbf{k}\mathbf{k}'}_{\nu\nu'}(\mathbf{q}+\mathbf{G})B^{\mathbf{k}\mathbf{k}'*}_{\mu\nu'}(\mathbf{q}+\mathbf{G})}{|\mathbf{q}+\mathbf{G}|^2}, \tag{25}$$

$$\Sigma^C_{\nu\mu}(\mathbf{k};\hbar z) = \frac{4\pi e^2}{\Omega}\sum_{\nu',\mathbf{k}'}\sum_{\mathbf{q},\mathbf{G}\mathbf{G}'} \times \frac{B^{\mathbf{k}\mathbf{k}'}_{\nu\nu'}(\mathbf{q}+\mathbf{G})B^{\mathbf{k}\mathbf{k}'*}_{\mu\nu'}(\mathbf{q}+\mathbf{G}')}{|\mathbf{q}+\mathbf{G}||\mathbf{q}+\mathbf{G}'|}\hbar \times \int_0^{\infty}\frac{d\omega}{\pi}\frac{\mathrm{Im}[\varepsilon^{-1}(\mathbf{q}+\mathbf{G},\mathbf{q}+\mathbf{G}';\omega)]}{\varepsilon^{\mathrm{QP}}_{\nu'}(\mathbf{k}') - \hbar z + \hbar\omega\,\mathrm{sgn}(\varepsilon^{\mathrm{QP}}_{\nu'}(\mathbf{k}')-\mu)}. \tag{26}$$

The Coulomb singularity in Eqs. (25) and (26) for $\mathbf{G}=\mathbf{G}'=0$ and $\mathbf{q}\to 0$ is treated according to previous suggestions.[48]

The partitioning of the self-energy into an exchange and a correlation term in Eqs. (25) and (26) is very convenient if dealing with a spectral representation on the real, positive frequency axis. However, for approximate screening functions, e.g., the plasmon-pole approximation or a static approximation,[31] it is more common to split the self-energy in a Coulomb-hole and a screened-exchange part, $\Sigma=\Sigma^{COH}+\Sigma^{SEX}+\Sigma^{DYN}$.[27] In the limit of static screening one finds for the self-energy[30]

$$\Sigma^{SEX}_{\nu\mu}(\mathbf{k}) = -\frac{4\pi e^2}{\Omega}\sum_{\nu',\mathbf{k}'}^{occ}\sum_{\mathbf{q},\mathbf{G}\mathbf{G}'} \frac{B^{\mathbf{k}\mathbf{k}'}_{\nu\nu'}(\mathbf{q}+\mathbf{G})B^{\mathbf{k}\mathbf{k}'*}_{\mu\nu'}(\mathbf{q}+\mathbf{G}')}{|\mathbf{q}+\mathbf{G}||\mathbf{q}+\mathbf{G}'|}\varepsilon^{-1}(\mathbf{q}+\mathbf{G},\mathbf{q}+\mathbf{G}';0), \tag{27}$$

$$\Sigma^{COH}_{\nu\mu}(\mathbf{k}) = \frac{2\pi e^2}{\Omega}\sum_{\mathbf{q},\mathbf{G}\mathbf{G}'}\frac{B^{\mathbf{k}\mathbf{k}}_{\nu\mu}(\mathbf{G}-\mathbf{G}')}{|\mathbf{q}+\mathbf{G}||\mathbf{q}+\mathbf{G}'|}\{\varepsilon^{-1}(\mathbf{q}+\mathbf{G},\mathbf{q}+\mathbf{G}';0) - \delta_{\mathbf{G}\mathbf{G}'}\}. \tag{28}$$

The static expression is obtained by setting $\hbar z=\varepsilon^{\mathrm{QP}}_{\nu'}(\mathbf{k}')$ in the denominator of Eq. (26). We used the completeness of the KS eigenfunctions to arrive at the explicit form (28) of the COH term. This is an important point because numerically the convergence with respect to the intermediate states is hard to reach for the COH part. The dynamical contribution to the self-energy follows from the correlation part (26) by subtracting the static limit as

$$\Sigma^{DYN}_{\nu\mu}(\mathbf{k};\hbar z) = -\frac{4\pi e^2}{\Omega}\sum_{\nu',\mathbf{k}'}\sum_{\mathbf{q},\mathbf{G}\mathbf{G}'}\frac{B^{\mathbf{k}\mathbf{k}'}_{\nu\nu'}(\mathbf{q}+\mathbf{G})B^{\mathbf{k}\mathbf{k}'*}_{\mu\nu'}(\mathbf{q}+\mathbf{G}')}{|\mathbf{q}+\mathbf{G}||\mathbf{q}+\mathbf{G}'|}$$

$$\times \int_0^\infty \frac{d\omega}{\omega\pi} \frac{\mathrm{Im}[\varepsilon^{-1}(\mathbf{q}+\mathbf{G},\mathbf{q}+\mathbf{G}';\omega)][\varepsilon_{\nu'}^{\mathrm{QP}}(\mathbf{k}') - \hbar z]}{[\varepsilon_{\nu'}^{\mathrm{QP}}(\mathbf{k}') - \hbar z + \hbar\omega\ \mathrm{sgn}(\varepsilon_{\nu'}^{\mathrm{QP}}(\mathbf{k}') - \mu)]\ \mathrm{sgn}(\varepsilon_{\nu'}^{\mathrm{QP}}(\mathbf{k}') - \mu)}. \tag{29}$$

Only the dynamical contribution (29) to the total XC self-energy requires one to sum over all intermediate (occupied and empty) states. This is advantageous from a numerical point of view, since the self-energy Σ is dominated by the static COH and SEX contributions (27) and (28). We evaluate the frequency integral in the dynamical contribution (29) at 250 mesh points with a spacing of 0.2 eV up to an energy of $\hbar\omega$=50 eV. Above this energy threshold the spacing is increased in such a way that another 150 mesh points are applied to perform the frequency integration between 50 and 150 eV. This ensures complete convergence for the molecules considered. It means that the dielectric matrix (23) has to be calculated and inverted for 400 frequencies to compute one integral. The number of reciprocal lattice vectors $\mathbf{G}$ and $\mathbf{G}'$ used in the computations of the three self-energy contributions (27)–(29) is another numerical and, hence, convergence issue. It is correlated with the number of electronic states. The number of bands c, ν in the dielectric matrix (23) should roughly be twice the number of $\mathbf{G}$ vectors for converged quasiparticle calculations.[31,32]

D. Pair excitation energies

Excitation energies obtained within the quasiparticle formalism describe single-particle excitations such as involved in direct or inverse photoemission experiments. For the description of the optical absorption, however, one has to go beyond the single-quasiparticle approximation. Spin-singlet pair excitations as measured in optical spectroscopies are described by the poles of the macroscopic, frequency-dependent dielectric function. This function is related to the microscopic dielectric matrix in the optical limit $\mathbf{q}\to 0$ ($\hat{\mathbf{q}}=\mathbf{q}/|\mathbf{q}|$) by[70,71]

$$\varepsilon_M(\hat{\mathbf{q}},\omega) = \hat{\mathbf{q}}\hat{\varepsilon}_M(\omega)\hat{\mathbf{q}} = \lim_{\mathbf{q}\to 0} \frac{1}{\varepsilon^{-1}(\mathbf{q}+\mathbf{G},\mathbf{q}+\mathbf{G}',\omega)}\bigg|_{\mathbf{G}=\mathbf{G}'=0}. \tag{30}$$

This function contains local-field effects defined as the difference between Eq. (30) and the $\mathbf{G}=\mathbf{G}'=0$ head element $\lim_{\mathbf{q}\to 0}\varepsilon(\mathbf{q},\mathbf{q};\omega)$ of the microscopic matrix, but no excitonic effects.

Approximating exchange and correlation within the GW approach (12), the kernel $\delta\Sigma(12)/\delta G(45)$ in the integral equation (7) is approximately given by $\sim W(1^+2)\delta(1-4)\delta(2-5)$.[30] The combination of Eqs. (6) and (7) then leads to a Bethe-Salpeter equation of the form $P=P_0-P_0WP$. The optical properties are, however, described by the polarization function $\bar{P}$ of the macroscopic dielectric function. Local-field effects can be included using[72,73]

$$\bar{P} = P_0 + P_0(\bar{v} - W)\bar{P}. \tag{31}$$

The bare Coulomb potential without its long-range part mediates the electron-hole exchange interaction,[29,30] where P_0 [Eq. (11)] represents the polarization function in independent-quasiparticle approximation. The attractive screened Coulomb interaction W in the Bethe-Salpeter equation (31) is usually approximated by its static limit. This is justified for electron-hole binding energies that are small compared to the lowest pair energy of the system.[30] Moreover, for the spectral properties it has been shown[74,75] that the dynamical effects in electron-hole screening and the one-particle Green's function in P_0 tend to cancel each other.

Using these approximations, the tensor elements of the macroscopic dielectric function can be rewritten in the Bloch-Fourier representation (using the KS eigenfunctions). The polarization function $\bar{P}$ of the macroscopic dielectric function may then be obtained via inverting an effective two-particle (in general: non-Hermitian) Hamiltonian reduced by the photon energy.[38,56] If the nonparticle conserving contributions to the Coulomb interaction as well as the coupling between the resonant and antiresonant contributions are neglected, one obtains for the tensor elements

$$\varepsilon_{ij}^M(\omega) = \delta_{ij} - \frac{8\pi e^2\hbar^2}{\Omega} \times \sum_{c,v,\mathbf{k}} \sum_{c',v',\mathbf{k}'} \{M_{cv}^{i^*}(\mathbf{k}) M_{c'v'}^j(\mathbf{k}') \bar{P}(cv\mathbf{k},c'v'\mathbf{k}';\omega) + \mathrm{c.c.\ and}\ \omega\leftrightarrow-\omega\}, \tag{32}$$

with the matrix elements of the velocity operator $\mathbf{v}$

$$M_{cv}^j(\mathbf{k}) = \frac{1}{\varepsilon_c(\mathbf{k}) - \varepsilon_v(\mathbf{k})} \int d^3\mathbf{x}\, \psi_{c\mathbf{k}}^*(\mathbf{x}) v_j \psi_{v\mathbf{k}}(\mathbf{x}). \tag{33}$$

The sums in Eq. (32) run over pairs of electrons in empty states c and holes in occupied (in the ground state) valence states v. The polarization function $\bar{P}$ obeys a BSE of the form

$$\sum_{c'',v'',\mathbf{k}''} \{\hat{H}(cv\mathbf{k},c''v''\mathbf{k}'') - \hbar(\omega + i\gamma)\delta_{cc''}\delta_{vv''}\delta_{\mathbf{kk}''}\}\bar{P}(c''v''\mathbf{k}'',c'v'\mathbf{k}';\omega) = -\delta_{cc'}\delta_{vv'}\delta_{\mathbf{kk}'}, \tag{34}$$

where $\hbar\gamma$ represents the damping energy. The effective electron-hole pair Hamiltonian of excited electrons and holes, more precisely quasielectrons and quasiholes, is given by[29,37,73]

$$\hat{H}(cv\mathbf{k},c'v'\mathbf{k}') = [\varepsilon_c^{\mathrm{QP}}(\mathbf{k}) - \varepsilon_v^{\mathrm{QP}}(\mathbf{k})]\delta_{cc'}\delta_{vv'}\delta_{\mathbf{kk}'}$$

$$-\frac{4\pi e^2}{\Omega}\sum_{\mathbf{q}}\sum_{\mathbf{G},\mathbf{G}'}\frac{B^{\mathbf{k}\mathbf{k}'}_{cc'}(\mathbf{q}+\mathbf{G})B^{*\mathbf{k}\mathbf{k}'}_{vv'}(\mathbf{q}+\mathbf{G}')}{|\mathbf{q}+\mathbf{G}||\mathbf{q}+\mathbf{G}'|}\varepsilon^{-1}(\mathbf{q}+\mathbf{G},\mathbf{q}+\mathbf{G}';0)$$

$$+\frac{8\pi e^2}{\Omega}\sum_{\mathbf{q}}{\sum_{\mathbf{G}}}'\frac{B^{\mathbf{k}\mathbf{k}}_{cv}(\mathbf{q}+\mathbf{G})B^{*\mathbf{k}'\mathbf{k}'}_{c'v'}(\mathbf{q}+\mathbf{G})}{|\mathbf{q}+\mathbf{G}|^2}. \quad (35)$$

Our calculations for molecules show that in contrast to the static contributions to the XC self-energy (27) and (28), contributions due to the off-diagonal elements of the inverse dielectric function in the statically screened electron-hole attraction [second right-hand side (rhs) term] are nearly negligible. The Coulomb singularity in the screened electron-hole attraction of Eq. (35) is treated as in the XC self-energy. The pair Hamiltonian (35) describes spin-singlet excitations. If the third rhs term is not included, spin-triplet excitations are obtained.

For molecules the numbers of empty (c) and occupied (v) bands are small, in particular if low-energy optical excitations are considered, which do not lead to photoionization. Moreover, since one $\mathbf{k}$ point is sufficient for the BZ sampling, the polarization function $\bar{P}$ in Eq. (32) is easily obtained by diagonalizing the eigenvalue problem of the pair Hamiltonian (35).[36,38] For larger systems, a time-evolution approach suggested by our group[37,76] has been shown to lead to identical results.

III. MONOSILANE: NUMERICS AND RESULTS

A. Numerical details

Monosilane, SiH_4, is used to probe the dependence of the excitation energies on the details of the implementation. The ground-state calculations are performed as described in Sec. II A. Assuming T_d symmetry, i.e., H-Si-H angles equal to the tetrahedron angle, we obtain a Si-H bond length of 1.477 Å, only slightly below the measured 1.481 Å. Previous calculations[56,77] slightly overestimated the bond lengths.

The number of $\mathbf{G}$ vectors needed for convergence can be estimated by a Hartree-Fock calculation with $\varepsilon(\mathbf{q}+\mathbf{G},\mathbf{q}+\mathbf{G}';\omega)=\delta_{\mathbf{G}\mathbf{G}'}$. We find an energy-cutoff $\hbar^2/2m\mathbf{G}^2$ of 6 Ry to be sufficient. The Fock operator (25) is then converged with a residual error of less than 0.05 eV. Though 6 Ry is a rather small cutoff value, the number of $\mathbf{G}$ vectors in the sums (27), (28), and (35) can be appreciable. It is about 2500 for a SiH_4 molecule in a 11.9 Å single cubic (sc) supercell. Considerably more $\mathbf{G}$ vectors need to be taken into account for larger molecules that require larger supercells. To check the influence of the number of bands needed for numerical completeness, we tested the validity of the relation between Bloch integrals (21)

$$B^{\mathbf{k}\mathbf{k}}_{\nu\nu}(\mathbf{G}-\mathbf{G}')=\sum_{\nu',\mathbf{k}'}B^{\mathbf{k}\mathbf{k}'}_{\nu\nu'}(\mathbf{G})B^{\mathbf{k}\mathbf{k}'*}_{\nu\nu'}(\mathbf{G}') \quad (36)$$

for the molecular orbitals of SiH_4. Figure 1 shows the rhs of Eq. (36) for the lowest occupied molecular state of SiH_4 as a function of the length of $\mathbf{G}$, ($\mathbf{G}'=\mathbf{G}$) for different numbers of molecular states. Completeness is clearly not achieved for large $\mathbf{G}$ even for a large number of intermediate states. In the case of SiH_4, we take $\mathbf{G}$ vectors up to an absolute value of $8.3\times 2\pi/a_s$ into account. Even for 1024 reference bands one is far from completeness, the Bloch integral for the lowest molecule orbital is not converged for large $\mathbf{G}$ vectors. The situation is even worse for less localized molecule orbitals at higher energy. Large $\mathbf{G}$ vectors require more than 5000 reference states for fulfilling the completeness. This number of states is computationally demanding even for ground-state calculations and restricts the calculations to relatively small systems.

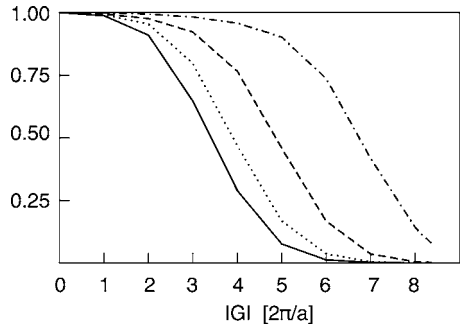

FIG. 1. Square of the Bloch integral (21) of the lowest SiH_4 molecule state calculated via the sum (36) in dependence on the size of the $\mathbf{G}$ vector. Solid, dotted, dashed, and dash-dotted lines show results for 16, 64, 256, and 1024 intermediate states. A supercell with an edge length $a_s=11.9$ Å is used.

In Fig. 2 the influence of the number of intermediate molecule states on the quasiparticle energies is shown. Two methods are compared. In one approach the completeness of the KS eigenstates is exploited analytically. According to Eqs. (22) and (28), the sum over intermediate states only occurs in the dynamical contribution (29). In the second

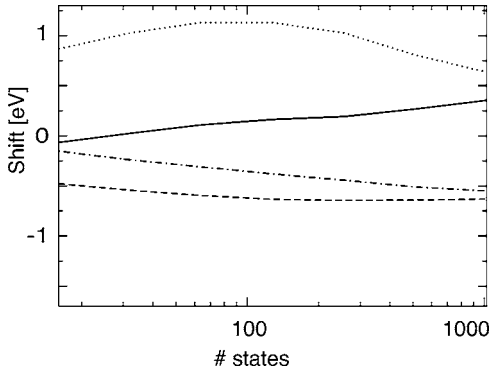

FIG. 2. Correlation contributions (26) to the SiH_4 quasiparticle shifts, $\langle\nu|\Sigma^C(\varepsilon^{\mathrm{QP}}_\nu)|\nu\rangle$, vs the number of intermediate states. The completeness relation has been exploited analytically, or the sum is performed numerically. Results for the HOMO (analytical/numerical) are shown by solid/dotted lines, the LUMO results (analytical/numerical) are shown by dashed/dot-dashed lines. The dielectric functions are calculated using KS eigenvalues.

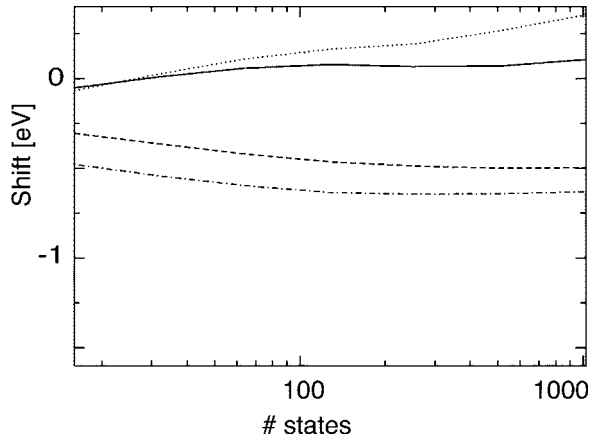

FIG. 3. Correlation contributions (26) to the SiH_4 quasiparticle shifts, $\langle \nu | \Sigma^C(\varepsilon_\nu^{\mathrm{QP}}) | \nu \rangle$, vs the number of intermediate states. The completeness relation has been exploited analytically. The eigenvalues in the dielectric matrix were taken to KS-like values or QP energies. Solid/dotted lines show the QP/KS results for the HOMO. Dashed/dash-dotted lines show the QP/KS results for the LUMO.

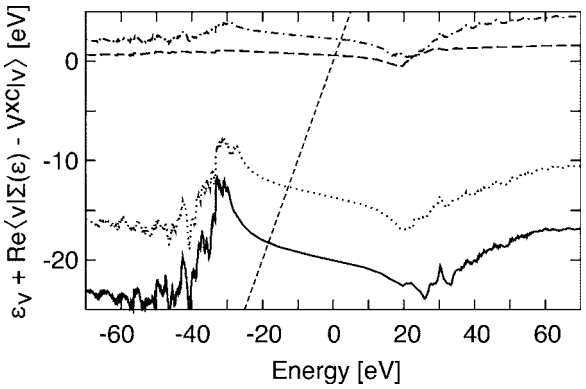

FIG. 4. Real part of the self-energy differences (18) added to the corresponding KS eigenvalues vs single-particle excitation energy. The dielectric function has been calculated with 256 bands. Solid, dotted, dashed, and dash-dotted lines represent the state 1 (HOMO-1), states 2,3,4 (HOMO), state 5 (LUMO), and states 6,7,8 (LUMO+1), respectively. The straight short-dashed line represents the linear function ε. The crossings with the other lines define the QP energies $\varepsilon_\nu^{\mathrm{QP}}$.

approach, the sum over intermediate states occurs also in the COH term. The energies of the highest occupied molecular orbital (HOMO) and the lowest unoccupied molecular orbital (LUMO) are considered. The analytical exploitation of the completeness leads to QP shifts that are almost converged for about 100 states. The second approach requires to take about ten times more states into account, in particular to achieve convergence for the HOMO. This is due to the COH operator that is very sensitive to the number of states. To reduce the numerical effort the completeness of the states is therefore exploited analytically wherever possible.

Another problem concerns the use of the QP energies in the self-energy expression (29) and in the screening function (23). In order to compute the shifts presented in Fig. 2, the dielectric matrix is calculated with KS eigenvalues and hence is not involved in the self-consistent determination of the QP eigenvalues. The true quasiparticle energies entering the dielectric function are much closer to the HF-like energies

$$\varepsilon_\nu^{\mathrm{HF}} = \varepsilon_\nu + \langle \nu | \Sigma^X - V^{XC} | \nu \rangle, \tag{37}$$

however, than to their KS analog. Here, Σ^X denotes the exchange self-energy operator (25). In Fig. 3we compare quasiparticle shifts for LUMO and HOMO of SiH_4, obtained using either KS or HF-like energies in the dielectric function. The dependence on the number of states is quite similar for both approximations. Discrepancies in the absolute values of the quasiparticle shifts are below 0.3 eV. However, due to the smaller screening of the dielectric function constructed from HF-like energies, the convergence with respect to the bands is improved. Consequently, we use $\varepsilon_v^{\mathrm{HF}}$ as start values for $\varepsilon_v^{\mathrm{QP}}$ throughout the paper.

The self-consistency condition (18) for the QP energies in conjunction with the large QP shifts suggests to investigate the energy dependence of the self-energy. In Fig. 4 we present the real diagonal part of the self-energy calculated by means of Eqs. (27)–(29). The self-energy is a smooth function of the energy for all orbitals between single-particle excitation energies from −25 to 20 eV. For larger positive or negative energies, however, one observes satellite structures corresponding to shake-off and shake-up excitations in the spectral function of the molecular system, the energies of which are defined as the poles of the density-density response function. In bulk systems these excitations are dominated by plasmons of the electron gas. The energy derivative $\beta_\nu = -\partial / \partial \varepsilon \, \mathrm{Re}\, \Sigma_{\nu\nu}(\varepsilon)|_{\varepsilon_\nu^{\mathrm{QP}}}$ of the self-energy between −20 and 10 eV is nearly constant and amounts to 0.13 for the occupied orbitals, while for the unoccupied orbitals a much weaker energy variation of less than 0.04 appears. This difference is mainly due to the reduced interaction, spatially and energetically, of an excitation in an unoccupied orbital with the electron density. This results in a reduced overlap of the wave functions and, therefore, smaller matrix elements. In addition, the larger energy differences in Eq. (29) reduce the effective dynamical screening. The quasiparticle energies are derived from the intersection $\varepsilon = \varepsilon_\nu^{\mathrm{QP}}$ of $\varepsilon_\nu + \mathrm{Re}\langle v | \Sigma(\varepsilon) - V^{XC} | v \rangle$ with the straight line ε. Numerically an iteration is used to determine the QP energies. In the cases studied here, the iteration always converges for starting values between −25 and 20 eV.

B. Quasiparticle energies

The real and imaginary parts of the energy-dependent self-energy can be also used to construct the spectral function of the quasiparticle Green's function. The spectral representation of the Green's function reads

$$G_{\nu\nu}(z) = \int_{-\infty}^{+\infty} \frac{d\omega}{2\pi} \frac{A_{\nu\nu}(\omega)}{z - \omega}. \tag{38}$$

The spectral function in diagonal approximation is given by ($\delta\Sigma = \Sigma - V^{XC}$)

$$A_{\nu\nu}(\omega) = i\{G_{\nu\nu}(\omega + i\eta) - G_{\nu\nu}(\omega - i\eta)\} = \frac{2|\mathrm{Im}\ \delta\Sigma_{\nu\nu}(\hbar(\omega \pm i\eta))|}{[\hbar\omega - \varepsilon_\nu - \mathrm{Re}\ \delta\Sigma_{\nu\nu}(\hbar(\omega \pm i\eta))]^2 + [\mathrm{Im}\ \delta\Sigma_{\nu\nu}(\hbar(\omega \pm i\eta))]^2}. \quad (39)$$

It is shown in Fig. 5.The line shape is largely determined by the energy variation of the imaginary part of the self-energy, which nearly vanishes between −20 and 10 eV for silane. The vanishing imaginary part of the self-energy leads to a sharp quasiparticle peak in the spectral function at the quasiparticle energy $\varepsilon_\nu^{\mathrm{QP}}$. The reciprocal linewidth of this quasiparticle peak corresponds to the lifetime of the quasiparticle. The actual spectral weights of the quasiparticle peaks depend on the considered system and the state occupation. For molecules we find that more than 80% of the spectral weight is accumulated in the quasiparticle peak for occupied orbitals and even more for empty molecular states. Moreover, the electronic quasiparticles (defined by the sharp main peaks in Fig. 5) are only weakly damped. These findings *a posteriori* justify the approximations made so far to describe molecular excitations.

Quasiparticle energies obtained within several approximations are listed in Table I. In this table we give the KS eigenvalues ε_ν, the HF-like energies $\varepsilon_\nu^{\mathrm{HF}}$ [Eq. (37)], and QP energies $\varepsilon_\nu^{\mathrm{QP}}$ for different approaches to describe the screening in the SiH_4 system. The quasiparticle energies were obtained iteratively from Eq. (18). Self-consistency is achieved after four iterations starting from both KS- or HF-like eigenvalues. The first column contains the KS energies of SiH_4, where the HOMO of t_2 symmetry ($\nu=2,3,4$) and the LUMO+1 ($\nu=6,7,8$) are triply degenerate, while the LUMO of a_1 symmetry ($\nu=5$) and the lowest occupied molecular orbital ($\nu=1$) are nondegenerate. The HOMO-LUMO gap amounts to 7.92 eV. The last column contains the values that have been calculated with a vacuum screening, i.e., $W=\nu$, which is equivalent to the Hartree-Fock approximation for the XC self-energy $\Sigma=\Sigma^X$. In the HF case the HOMO-LUMO gap amounts to 13.9 eV. The quasiparticle energies calculated for different approximations of the screening are between these two extremes. The second and third column denoted with DYN(KS) and DYN(HF) show QP values which are self-consistently computed by means of Eqs. (27)–(29) but with either Kohn-Sham or Hartree-Fock-like energies in the dielectric function, as described above. Compared to the KS values, the HOMO energy is significantly lowered in energy by more than 4 eV, while the LUMO position is shifted to higher energies by more than 1 eV. The quasiparticle corrections thus increase the HOMO-LUMO gap by about 5 eV. The comparison of the self-consistently obtained QP values, DYN(HF), with values from a static screening calculation, STAT (column 4), exhibits significant differences for HOMO and HOMO-1, while the values for the unoccupied orbitals remain nearly the same. The large differences between static and frequency-dependent calculations show the importance of the dynamics of the screening. The static-screening limit also allows for testing the frequency integration in Eq. (26) or Eq. (29) by setting $\hbar z = \varepsilon_{\nu'}^{\mathrm{QP}}(\mathbf{k}')$ in the energy denominators. The result of this calculation in the fifth column, STAT*, is nearly indistinguishable from the true static calculation, STAT. This proves that the frequency integration in Eqs. (26) and (29) is converged and numerically stable. The DIAG column in Table I is obtained by using a diagonal inverse dielectric function with $\mathbf{G}=\mathbf{G}'$. We know from crystals and surfaces that diagonal dielectric functions, even model dielectric functions, are in many instances sufficient for GW self-energy calculations.[37,44,48]. This does not hold for molecules, where the result for diagonal screening is close to the case of no screening at all.

The QP eigenvalues resulting for single-particle excitations in the silane molecule in Table I may be compared with earlier calculations and experimental data. The diagonal DYN(HF) approach that is the most accurate method studied

TABLE I. Calculated SiH_4 quasiparticle energies in eV for different approximations of the screening: DYN(KS) – full GWA but use of KS eigenvalues instead of QP energies in screening (23), DYN(HF) – full GWA but use of energies (40) instead of QP values in screening (23), STAT – neglect of dynamical screening, i.e., of the contribution (29), STAT* – neglect of dynamical screening by setting $\hbar z = \varepsilon_{\nu'}^{\mathrm{QP}}(\mathbf{k}')$ in Eq. (26), DIAG – full GW approximation as DYN(HF) but neglecting the local-field contributions $\mathbf{G} \neq \mathbf{G}'$ to the screening in Eqs. (27)–(29). In all cases, the diagonal approach (20) has been applied and the dielectric matrix is constructed from 1024 bands and HF-like energies (40). The QP energies are compared with the KS eigenvalues and the HF-like energies, $\Sigma=\Sigma^X$.

State	KS	QP					HF
		DYN(KS)	DYN(HF)	STAT	STAT*	DIAG	
1	−13.45	−17.40	−18.26	−19.62	−19.65	−19.49	−19.67
2,3,4	−8.42	−12.41	−12.67	−13.55	−13.58	−12.65	−12.77
5	−0.50	0.50	0.63	0.56	0.59	0.91	1.13
6,7,8	−0.04	1.95	2.23	2.07	2.11	3.24	3.43
HOMO-LUMO gap	7.92	12.91	13.30	14.01	14.07	13.40	13.90

TABLE II. Calculated SiH_4 quasiparticle Hamiltonian $\delta_{\nu,\nu'}[\varepsilon_\nu+\langle\nu|\Sigma(\varepsilon_\nu^{\mathrm{QP}})-V^{XC}|\nu\rangle]+(1-\delta_{\nu\nu'})\langle\nu|\Sigma^{COH}+\Sigma^{SEX}-V^{XC}|\nu'\rangle$ in eV for the first 12 states. The upper triangle and the diagonal contain the real parts of the elements of the Hermitian matrix, the lower triangle represents the imaginary parts of the self-energy matrix elements.

State	1	2	3	4	5	6	7	8	9	10	11	12
1	−18.257	0.002	−0.001	−0.001	0.563	0.003	0.000	−0.006	−0.423	0.012	0.036	0.014
2	0.003	−12.666	0.000	−0.001	−0.001	0.011	−0.001	0.001	0.003	0.328	0.028	−0.028
3	−0.001	0.000	−12.668	0.000	−0.001	0.001	0.006	−0.001	0.003	0.034	−0.071	0.310
4	0.002	−0.002	0.000	−12.665	0.001	−0.003	−0.003	0.004	0.033	−0.020	0.338	0.071
5	−0.052	0.000	0.000	0.000	0.633	−0.023	−0.001	0.029	−1.296	0.017	0.133	0.043
6	−0.001	−0.001	0.000	0.001	0.001	2.164	0.012	0.006	0.001	0.335	−0.033	−0.045
7	0.000	0.001	−0.006	0.003	0.002	−0.011	2.223	0.034	0.010	0.026	−0.078	0.429
8	0.000	0.001	0.000	−0.001	−0.002	−0.002	0.042	2.320	0.077	0.164	0.661	0.414
9	−0.102	0.005	0.001	0.008	−0.440	0.008	0.018	0.040	1.187	−0.002	−0.007	0.001
10	−0.003	0.108	0.000	−0.003	−0.013	0.157	0.037	0.041	0.005	1.369	0.025	0.021
11	−0.002	0.004	−0.001	−0.013	0.005	−0.037	−0.084	0.079	0.002	−0.007	1.418	0.061
12	−0.007	0.001	−0.133	−0.033	−0.016	−0.010	0.238	−0.095	−0.001	−0.012	−0.021	1.415

here gives −12.67 eV for the HOMO and 0.6 eV for the LUMO. Other GW calculations find values −12.7 and 1.1 eV.[55,78] A quantum Monte Carlo simulation[78] leads to values of −12.6 and 0.2 eV. DFT calculations[79] that use the asymptotically accurate exchange-correlation functionals due to Leeuwen and Baerends (LB94)[80] or Casida and Salahub (ACLDA)[81] predict HOMO values of −12.9 and −12.2 eV, respectively. The experimental value for the ionization energy (i.e., $-\varepsilon_{\mathrm{HOMO}}^{\mathrm{QP}}$) is 12.6 eV.[82] Other experimentalists report a broad peak at 11.5–13.5 eV in the photoemission spectrum of SiH_4 (cf. discussion in Ref. 56).

C. Beyond first-order perturbation theory

We now drop the restriction to diagonal self-energies $\Sigma_{\nu\nu}(\varepsilon)$ and take the nondiagonal elements of Eqs. (27) and (28) into account. To reduce the numerical effort, we calculate the diagonal elements self-consistently as described above, but obtain the off-diagonal elements in the static approximation, i.e., account for the SEX and COH contributions (27) and (28) but neglect the dynamical contribution (29). This approximation can be made because the off-diagonal elements, in particular their frequency-dependent parts, are smaller than the diagonal elements. This is illustrated by the numerical results for the calculated quasiparticle matrix for the 12 lowest molecule states $\varepsilon_\nu\delta_{\nu\mu}+\Delta_{\nu\mu}$ with $\Delta_{\nu\nu}=\mathrm{Re}\langle v|\Sigma(\varepsilon_v^{\mathrm{QP}})-V^{XC}|v\rangle$ and $\Delta_{\nu\mu}=\mathrm{Re}\langle v|\Sigma^{SEX}+\Sigma^{COH}-V^{XC}|\mu\rangle$ in Table II.A supercell with an edge length of 11.9 Å has been used. The first four states are occupied bonding orbitals and the next four states are unoccupied antibonding orbitals. The states above these eight orbitals are scattering states that are strongly affected by the supercell size. Note that the diagonal quasiparticle energies of the states nine and ten are energetically below the states six to eight, while the corresponding KS values were above. Hence the energetic order of the bands, commonly preserved during a quasiparticle calculation, is changed. This is rather independent of the numerical details and occurs already in the HF-like approximation $\varepsilon_\nu^{\mathrm{HF}}$ [Eq. (37)]. Most off-diagonal elements are small compared to the diagonal elements of the operator $\Sigma(\varepsilon)-V^{XC}$. There is, however, one exception. The interaction of the LUMO with the first scattering state is quite large (at least for the 11.9 Å supercell) and leads to their strong interaction and hence mixing. This was also observed by the authors of Ref. 36.

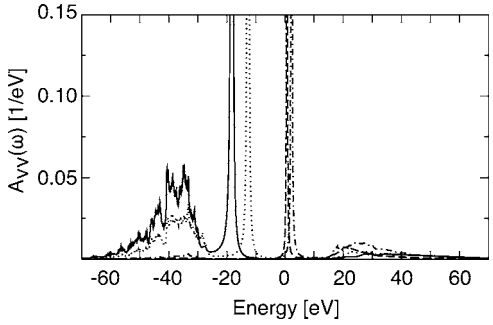

FIG. 5. Spectral function (39) of the quasiparticle Green's function. The shake-up satellite structures are clearly visible. Solid, dotted, dashed, and dash-dotted lines represent state 1 (HOMO-1), states 2, 3, 4 (HOMO), state 5 (LUMO), and states 6, 2, 8 (LUMO+1), respectively.

To obtain the true quasiparticle energies and wave functions, the eigenvalue problem (16) must be diagonalized. The result (restricted to bonding and antibonding orbitals only) is listed in Table III. Compared to the diagonal energies of Table II, the eigenvalues are only slightly shifted. Furthermore, the matrix formed by the eigenvectors is practically diagonal. Thus we find that the quasiparticle wave functions are almost equal to the KS wave functions. There seems to be one exception. The degenerate orbitals two, three, and four, forming the HOMO, are mixed in their subspace upon diagonalization. However, this is only a numerical artifact. The original character of the KS orbitals is shown in Figs. 6(a)–6(c). Though they are degenerate in energy, the orbitals do not have the symmetry of the molecule. The corresponding quasiparticle orbitals are obtained as a linear combina-

TABLE III. Eigenvalues in eV and eigenvectors of the quasiparticle matrix in Table II for the first eight QP states.

State	Eigenvalue	Eigenvector							
1	−18.27	0.9996	0.0006	0.0002	0.0005	0.0299	0.0002	0.0000	0.0003
2	−12.66	0.0006	0.4184	0.8290	0.3711	0.0000	0.0002	0.0006	0.0002
3	−12.66	0.0005	0.6601	0.5384	0.5238	0.0001	0.0004	0.0002	0.0002
4	−12.66	0.0001	0.6239	0.1511	0.7667	0.0001	0.0006	0.0003	0.0002
5	0.64	0.0299	0.0001	0.0001	0.0000	0.9993	0.0154	0.0018	0.0175
6	2.16	0.0002	0.0007	0.0001	0.0001	0.0129	0.9487	0.3065	0.0766
7	2.20	0.0002	0.0001	0.0006	0.0004	0.0134	0.3091	0.8585	0.4089
8	2.34	0.0002	0.0001	0.0002	0.0001	0.0142	0.0651	0.4110	0.9092

tion of these KS orbitals according to the eigenvectors in Table III. The resulting QP wave functions are nearly identical and show the T_d symmetry of the molecule [see Figs. 6(e)–6(g)]. The linear combination of the three KS orbitals only describes a subspace transformation.[83] The states 6, 7, and 8 in Table III are not degenerate. This is a consequence of the fact that the periodic arrangement of the SiH_4 molecules in sc supercells reduces the symmetry and affects less localized molecular states. The relatively minor influence of the diagonalization on the quasiparticle energies and wave functions also indicates a minor influence of the specific form of the XC correlation functional used in the DFT calculations on the final excitation energies.

If the diagonalization is done for more than the lowest eight molecule orbitals there occurs a strong interaction of the LUMO with the first scattering (ninth) state. Though the latter is not a bound state of the molecule, its wave function still overlaps with the LUMO, resulting in a non-negligible interaction. The eigenvalues of both states change according to $\tilde{\varepsilon}_{5,9}=(\varepsilon_5^{\mathrm{QP}}+\varepsilon_5^{\mathrm{QP}})/2\pm\sqrt{(\varepsilon_5^{\mathrm{QP}}-\varepsilon_9^{\mathrm{QP}})^2/4+|\mathrm{Re}\ \delta\Sigma_{59}|^2}$ with $\varepsilon_\nu^{\mathrm{QP}}$ as the diagonal QP energies, $\varepsilon_9^{\mathrm{QP}}-\varepsilon_5^{\mathrm{QP}}=0.55$ eV, and $|\mathrm{Re}\ \delta\Sigma_{59}|=1.30$ eV. Because of the mixing of the LUMO with the ninth state, the resulting quasiparticle orbital is less localized as shown in Figs. 6(d) and 6(h). Similar observations were made with scattering states even higher in energy. We come back to this problem further below.

D. Optical pair excitations

The calculated optical spectra are strongly influenced by many-body effects. However, they are also very sensitive with respect to the supercell size and description of the scattering states. We study these effects by calculating the optical absorption spectrum of silane, more precisely the imaginary part of its macroscopic dielectric function (32) in a supercell. Because of the high symmetry, only the diagonal element $\varepsilon^M(\omega)$ exists.

We start by calculating spectra in the approximation of independent KS particles, for which the pair Hamiltonian (35) is diagonal and given by $[\varepsilon_c(\mathbf{k})-\varepsilon_v(\mathbf{k})]$. Figure 7 shows the results for different supercell sizes. The two prominent peaks at 7.9 and 8.4 eV stem from the HOMO-LUMO and HOMO-LUMO+1 transitions, respectively. These peaks are almost identical for the four supercells. Only the lowest peak is slightly shifted by 0.1 eV towards higher photon energies due to the reduced binding of the LUMO state. However, convergence seems to be achieved for edge lengths of 15.9 Å. Above the ionization edge at about 8.5 eV, the spectrum is dominated by transitions into scattering states. They are strongly suppressed with increasing supercell size.

Figures 8 and 9 indicate clear limitations of the supercell approach. In Fig. 8 spectra are shown, where the off-diagonal elements of the XC self-energy are taken into account, but the electron-hole attraction is not included. Neglecting the scattering states, i.e., the quasicontinuum of states above $v=8$, the well-known two absorption peaks related to the HOMO-LUMO and HOMO-LUMO+1 transitions appear at 13.4 and 14.9 eV, respectively. They occur at 9.5 and 11.0 eV with electron-hole attraction (Fig. 9). We thus obtain a large exciton binding energy of about 3.9 eV in monosilane. This magnitude is in reasonable agreement with earlier

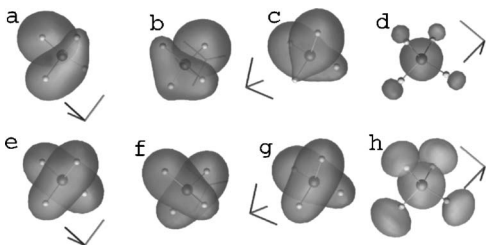

FIG. 6. Upper row: Squares of the degenerate KS HOMO orbitals of SiH_4 (a)–(c) and the KS LUMO (d). Lower row: corresponding QP wave functions of the HOMO orbitals (e)–(g) and the LUMO (h).

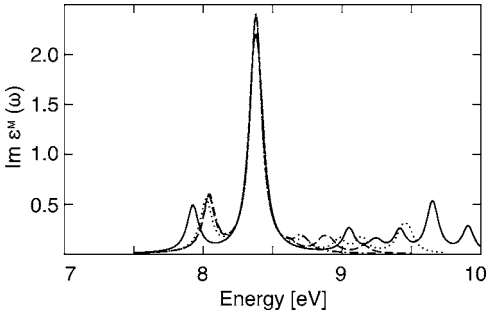

FIG. 7. SiH_4 absorption spectra calculated on the KS level of theory with 16 molecular states for different supercell sizes of 11.9 Å (solid line), 15.9 Å (dotted line), 19.8 Å (dashed line), and 35.5 Å (dash-dotted) line.

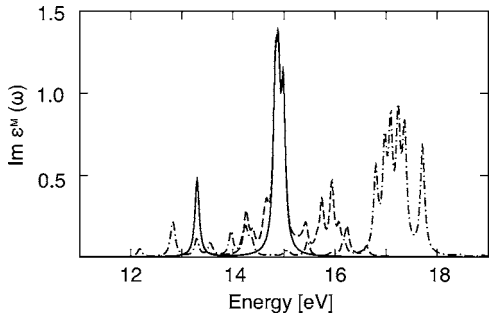

FIG. 8. SiH_4 absorption spectra calculated on the independent-quasiparticle level of theory. Solid line: 8 states, diagonal and full QP approach cannot be discriminated on the scale of the figure. Dashed/dash-dotted line: 32 states, diagonal/full (including off-diagonal elements) QP approach.

calculations.[84,85] The inclusion of scattering states with energies above the ionization edge and, in particular, their coupling via the off-diagonal elements does not only give rise to high-energy transitions. Rather, there is a tendency to redistribute the double-peak structure over more peaks, at least for a supercell size of $a_s=11.9$ Å. This effect is strongly reduced for larger supercells (not shown in Figs. 8 and 9). It is also reduced when the electron-hole attraction is included in the calculations (Fig. 9), because this increases the localization of the electron states. That this problematic issue arises in the first place is largely caused by the incorrect description of the continuum of scattering states in a supercell. The continuum becomes a quasicontinuum of eigenvalues with confined wave functions. The increase of the supercell size delocalizes these states and, hence, gives rise to smaller off-diagonal matrix elements of the XC self-energy.

In order to avoid the dilemma of the description of the scattering states in a supercell approach (that should also occur when representing these states by Gaussians[55]), we restrict our calculations to the optical absorption at relatively low photon energies and use large supercells, where the influence of scattering states on the low-energy spectra is suppressed. The latter effect is demonstrated in Fig. 10. Despite the inclusion of many scattering states, large supercells recover the two main absorption peaks known from the restriction to eight molecular states (Fig. 9). Here, the peak positions are blueshifted by about 0.5 eV because of the neglect of the screening, i.e., the use of $\varepsilon(\mathbf{q}+\mathbf{G},\mathbf{q}+\mathbf{G}';\omega)=\delta_{\mathbf{GG}'}$. As a consequence, in practical computations only the first eight molecule states may be taken into account. These states are below the ionization edge in KS approximation (cf. Table I). Of course, the localization of the empty QP states, in particular of the LUMO, is somewhat overestimated.[36] However, the Coulomb attraction of electrons and holes also localizes the electrons in the pair excitations. This behavior is schematically indicated (within the single-particle picture) in Fig. 11. The localization of the electron due to the electron-hole attraction gives an additional justification for restricting the number of states used in the calculations. The restriction to eight states, i.e., the neglect of the scattering states, leads to the spectrum of Fig. 12. Besides the two main peaks, which are still dominated by single-particle transitions, a small peak occurs in between. It is a consequence of the Coulomb attraction and hence cannot be understood in a single-particle picture. The measured positions of the three lowest absorption peaks of 8.8, 9.7, and 10.7 eV are not exactly repro-

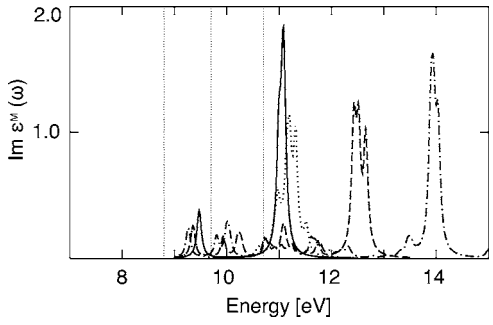

FIG. 9. SiH_4 absorption spectra calculated including both full quasiparticle corrections and electron-hole interaction. Solid, dotted, dashed, and dash-dotted lines represent the results obtained for 8, 12, 16, and 32 states, respectively. Vertical dotted lines indicate the experimental peak positions (Ref. 82).

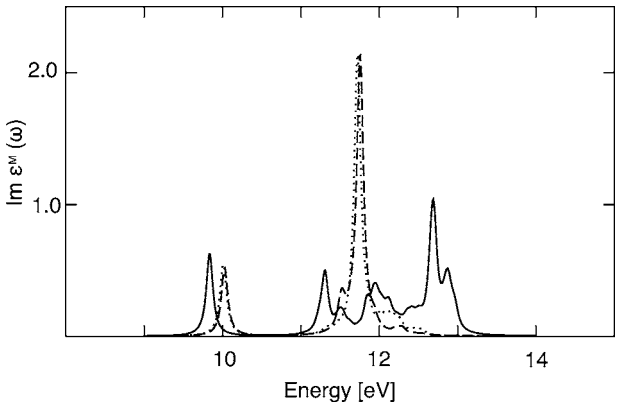

FIG. 10. Influence of the supercell size on the absorption spectrum of SiH_4 calculated by including both full QP corrections and the electron-hole interaction for 32 molecular states. Solid, dotted, and dashed lines show results obtained for $a_s=15.9$ Å, $a_s=31.8$ Å, and $a_s=47.6$ Å, respectively. In order to make the calculations numerically possible, the vacuum dielectric function $\varepsilon(\mathbf{q}+\mathbf{G},\mathbf{q}+\mathbf{G}';\omega)=\delta_{\mathbf{GG}'}$ was used, corresponding to a HF-like approach.

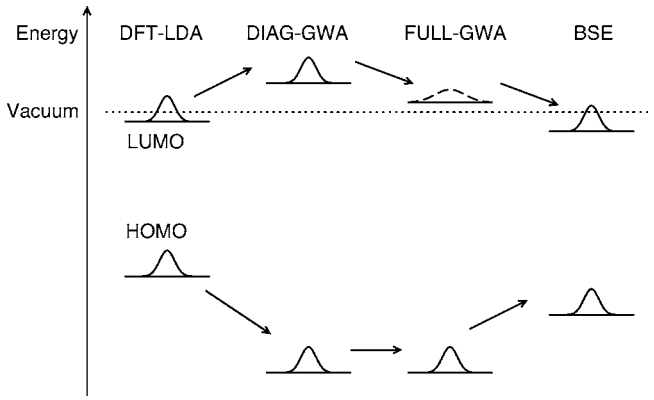

FIG. 11. Schematic representation of the localization of the HOMO and LUMO wave functions in different approximations for the electron-electron interaction.

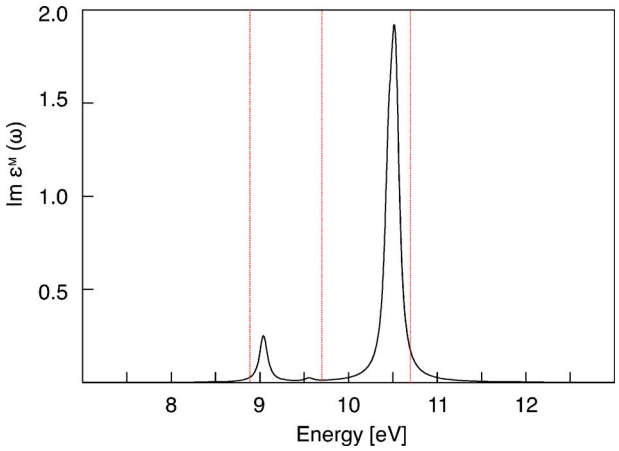

FIG. 12. (Color online) SiH_4 absorption spectrum calculated including both full quasiparticle corrections and electron-hole interaction for the lowest eight molecular orbitals. The vertical dotted lines indicate experimental peak positions (Ref. 82).

duced by the computed peak energies 9.0, 9.6, and 10.5 eV in Fig. 12. The maximum deviation of 0.2 eV indicates the accuracy that can be expected from the kind of calculations presented here. We observe, however, that increasing the supercell size shifts the transitions to higher energies. For supercells with $a_s=15.9$ Å values of 9.3, 9.7, and 10.7 eV are obtained. Our results agree relatively well, at least for the lowest transition, with the energies of 9.0, 10.2, and 11.2 eV computed in a previous work using a similar approach.[55] A quantum Monte Carlo calculation[85] leads to a value of 9.2 eV for the lowest pair excitation, again close to our result. The TDLDA calculations in Ref. 84 lead to somewhat lower excitation energies of 8.2, 9.2, and 9.7 eV, while the usage of the asymptotically corrected exchange-correlation functionals LB94/ACLDA results in values of 8.8/8.5, 9.5/9.3, and 10.8/10.3 eV, respectively.[86]

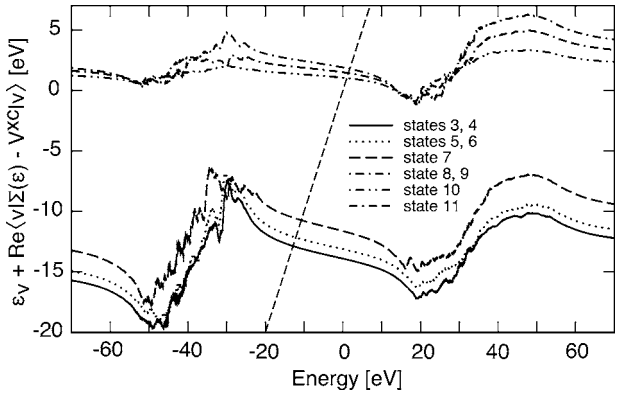

FIG. 13. Real part of the diagonal self-energy differences (18) added to the corresponding KS eigenvalues (see inset) vs single-particle excitation energy. The frequency-dependent dielectric matrix (23) has been computed including 512 states. The straight short-dashed line represents the linear function ε. The crossings with the other lines define the QP energies $\varepsilon_\nu^{\mathrm{QP}}$.

IV. APPLICATIONS TO OTHER MOLECULES

A. Disilane

Disilane, Si_2H_6, has D_{3d} symmetry in the ground state. We model it in a supercell with $a_s=13.8$ Å. Consequently, the number of **G** vectors in the **k**-space representation is increased to 4000. The bond lengths obtained are $d_{\mathrm{Si\text{-}Si}}=2.32$ Å and $d_{\mathrm{Si\text{-}H}}=1.49$ Å. 512 molecule states are used to compute the frequency-dependent dielectric matrix.

Disilane possesses 14 valence electrons and hence seven occupied molecule states. Their energy levels are given in Table IVtogether with those of the subsequent seven empty states. Within the KS approach, the first 11 levels are below the ionization edge. Test calculations for a larger supercell with $a_s=30$ Å yields similar results. Only the states 12/13 move slightly below (−0.03 eV) the vacuum energy. As a consequence of the lower symmetry, only nondegenerate or doubly degenerate states occur. The inclusion of the full GW self-energy (or the exchange term only, called HF-like) shifts the occupied (empty) levels towards lower (higher) energies. The quasiparticle shifts of the occupied (empty) states are of the order of −4 eV (1.5 eV). The shifts are larger by restricting the calculation to the exchange contributions. The effect of the off-diagonal elements of the XC self-energy is small. Only the states 14 and 8 mix. The absolute QP value of the HOMO (state 7) of 10.74 eV is very close to the measured ionization energy of 10.66 eV[82] and previous calculations[55] that obtained 10.6 eV.

The QP energies are again strongly influenced by the dynamical screening. This effect is indicated in Fig. 13. The energy variations are similar to the case of monosilane (Fig. 4). They are smoother, however, in the range of the satellite structures. This may already indicate that in larger molecules the isolated shake-up and shake-off excitations start to be replaced by the continuum of wave-vector-dependent plasmons typically for the solid. The variations are also smaller around the QP energies. The energy derivatives $\beta_\nu=-\partial/\partial\varepsilon\ \mathrm{Re}\,\Sigma_{\nu\nu}(\varepsilon)|_{\varepsilon=\varepsilon_\nu^{\mathrm{QP}}}$ are about 0.13 for the highest occupied states and almost vanish for the empty states. That means that only about 13% of the total spectral weight of the holes are related to the satellite structures while the spectral weight of the satellites practically vanishes for the electron excitation.

Optical absorption spectra of disilane calculated using 13 and 14 states are represented in Fig. 14. The self-energy effects (16) and the electron-hole interaction (35) are fully taken into account. Because of the increased number of molecule states with respect to monosilane, the spectrum above the absorption edge in Fig. 14 shows more peaks. The coupling of the KS states due to the off-diagonal elements $7\leftrightarrow14$ of the self-energy mainly influences the peaks around or above the photoionization limit. However, this coupling tends to reduce the spectral strengths of the transitions around 9 eV and to redistribute them towards higher energies. For photon energies below 10 eV, there are small peaks around 7.73 and 8.25 eV and a well-pronounced peak at 9.82 eV. With increasing number of states, the double-peak structure at 8.94/9.15 eV is redistributed to structures around 8.97 and 9.57 eV. Optical spin-singlet excitations have been

TABLE IV. Single-particle energy levels in eV of the lowest molecular states of Si_2H_6 in three different approximations, ε_ν, ε_ν^{QP}, and ε_ν^{HF} [Eq. (37)].

State	1	2	3/4	5/6	7	8	9	10/11	12/13	14
KS	−14.06	−12.39	−8.80	−8.11	−7.23	−0.63	−0.51	−0.65	0.12	0.21
QP	−18.75	−16.95	−12.86	12.10	−11.03	0.62	0.94	1.26	1.66	0.65
HF	−20.45	−18.23	−13.18	−12.37	−10.49	1.96	2.71	3.62	3.27	1.25

found experimentally[82] at 7.6, 8.4, 9.5, and 9.9 eV. Apart from the small additional structure somewhat below 9 eV, our calculated results well-describe the experimental findings. A similar many-body calculation but representing the KS eigenfunctions by Gaussians[55] yields peaks at 7.6, 9.0, and 9.6/9.8 eV in the energy range below $\hbar\omega=10$ eV. Depending on the choice of the exchange-correlation functional, TDDFT calculations predict the lowest two transition energies at 7.1–7.3 and 8.6–8.8 eV.[86]

B. Water

The water molecule is more polar and less symmetric than mono- and disilane. Its point group C_{2v} contains a rotation by 180° around the molecule axis and two mirror-symmetry operations. We model it in a supercell with $a_s=10$ Å. The real-space grid contains $64\times64\times64$ grid points. This suggests the use of 6000 **G** vectors for a converged quasiparticle calculation. The ground-state calculation within the DFT-GGA gives a length of the oxygen-hydrogen bonds of $d_{O\text{-}H}=0.966$ Å and an angle between the two bonds of 104.49°. The corresponding experimental values for gas-phase molecules are 0.957 Å and 104.47° (see data in Refs. 87 and 88).

According to the molecule symmetry, the atomic orbitals are derived from six linear combinations of a_1, a_2, b_1, and b_2 symmetry with nondegenerate energy levels. The eight valence electrons occupy the four lowest states. Results for the levels obtained by using different approximations for the electron-electron interaction are given in Table V.The highest molecular state considered here (state 6) is above the vacuum level already within DFT-GGA. This does not change if PAW pseudopotentials[63] and the VASP code[64] are used in the calculation. Only calculations for considerably larger supercells drag its energy below the vacuum level. However, it is numerically very expensive to perform quasiparticle and exciton calculations for supercell sizes of $a_s\approx20$ Å. When off-diagonal elements of the XC energy are considered, a coupling occurs only with the sixth molecular state. This can be expected to vanish for larger supercells.

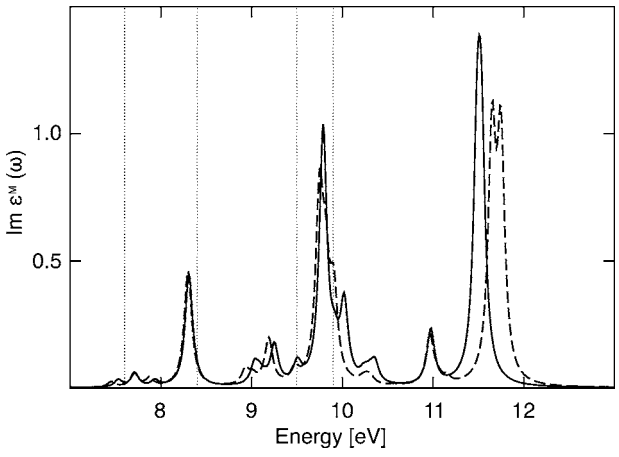

FIG. 14. Si_2H_6 absorption spectrum calculated including both quasiparticle corrections and electron-hole interaction for the lowest 13 (solid line) and 14 states (dashed line). The vertical dotted lines indicate experimental peak positions (Ref. 82).

The influence of the energy dependence of the screening on the QP energies is indicated in Fig. 15. It is most important for the occupied molecular states with $\beta_\nu=0.11(\nu=2,3,4)$, but nearly vanishes for the unoccupied states. The resulting QP eigenvalues in Table V are shifted towards negative (positive) energies for the occupied (empty) molecular states. The QP shifts vary between −7.7 and −4.7 eV (0.4 and 0.8 eV) for the occupied (empty) states. For the HF-like eigenvalues (37), these shifts with respect to the KS energies are again larger. Since the geometry of the H_2O molecule is fixed at the ground-state coordinates, the negative QP eigenvalues in Table V correspond to vertical ionization energies. We compare the resulting values with results of other calculations and measurements in Table VIfor the three highest occupied molecular levels $1b_2$, $3a_1$, and $1b_1$. Reference 59 is a modified QP approach that can be considered as a generalized GW Tamm-Dancoff approximation. It starts from a hybrid functional B3LYP within the DFT. The other work[89] is a outer-valence Green's function (OVGF) calculation. The underlying DFT calculations have been performed with Becke's exchange functional and Perdew's correlation functional. The theoretical results in Table VI agree with an accuracy of about 0.3 eV. The comparison of the calculated results with the measured values shows excellent agreement for the lower state 2 with b_2 symmetry. The agreement for the HOMO with b_1 symmetry is less convincing. The energy is underestimated by about 0.7 eV. We believe this is par-

TABLE V. Energy levels in eV of the six lowest molecular states of the H_2O molecule in four different approximations: ε_ν (from DFT-GGA), ε_ν^{QP} (from full and diagonal GW), and ε_ν^{HF} [Eq. (37)].

State	1	2	3	4	5	6
KS	−25.19	−13.11	−9.27	−7.21	−0.88	0.61
QP (diag.)	−32.93	−18.80	−14.42	−11.94	0.64	1.06
QP (full)	−32.95	−18.79	−14.42	−11.94	−0.13	1.83
HF	−36.92	−19.14	−15.47	−13.16	0.93	1.86

TABLE VI. The lowest vertical ionization energies of the H_2O molecule in eV from calculations (Refs. 59 and 89) and measurements (Refs. 90 and 91).

Molecular orbital	QP (this work)	QP (Ref. 59)	OVGF (Ref. 89)	Expt. (Ref. 90)	Expt. (Ref. 91)
$1b_1$	11.94	11.90	12.24	12.61	12.78
$3a_1$	14.42	14.18	14.51	14.73	14.83
$1b_2$	18.79	18.35	18.56	18.55	18.72

tially due to the DFT-GGA calculation using the 10 Å supercell: The KS eigenvalue is −7.21 eV (Table V), while other approaches[59] yield −7.63 eV. In general, however, we can conclude that the GW approximation gives excellent single-particle excitation energies also for H_2O. A scaling of the self-energy effects by a factor of 0.5 as observed for less sophisticated GW approaches[52] is not necessary.

The water molecule is optically anisotropic. Here we consider only the trace of the optical tensor (32), see Fig. 16. Whether or not the molecular state 6 is taken into account has an obvious influence on the high-energy region of the absorption spectrum. The HOMO-LUMO peak at about 7.2 eV results from strong excitonic effects: The redshift with respect to the corresponding QP peak of uncorrelated electron-hole pairs is about 5.2 eV. The excitonic effects thus largely compensate the blueshift of the KS position of the HOMO-LUMO transition of 6.3 eV. The strong excitonic effects in the water molecule are also indicated by an exciton radius of $R_{ex}=2.27$ Å (i.e., the average distance between electron and hole in the LUMO-HOMO pair), which we have calculated using the two-particle electron-hole wave function of the Hamiltonian (35) in real space. The hole is strongly localized at the oxygen atom of the molecule. Therefore the probability to find the electron of the pair has its maxima outside of the molecule that has a characteristic dimension of $d_{\mathrm{O-H}}\approx 1$ Å. The first three transitions (including six states) are obtained at 7.24, 9.62, and 10.07 eV for the 10 Å supercell. The experimentally reported transitions occur at 7.3–7.49 eV for the first, 9.69–9.73 eV for the second, and 9.99–10.10 eV for the third peak (cf. data collection in Ref. 92). The agreement between our results and the experiment is excellent. The GW/BSE method yields water optical excitation energies that are no less accurate than sophisticated *ab initio* quantum-chemical methods. A complete active space self-consistent field (CASSCF) calculation,[92] for example, predicts transition energies of 7.58, 9.80, and 10.45 eV. CC calculations are of comparable accuracy with 7.53 eV for the lowest singlet transition, whereas the corresponding value of 6.86 eV obtained from TDDFT in Ref. 93 is clearly below the experiment. However, similar to the case of monosilane, the usage of an asymptotically corrected exchange-correlation functional in the TDDFT leads to an increase of the excitation energies: Cai *et al.*[94] predict a value of 7.61 eV for the lowest transition.

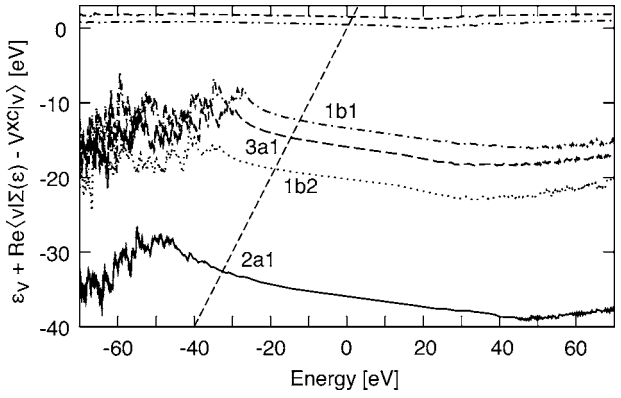

FIG. 15. Real part of the H_2O diagonal self-energy differences (18) added to the corresponding KS eigenvalues (see labels) vs single-particle excitation energy. The frequency-dependent dielectric matrix (23) has been computed including 260 states. The straight short-dashed line represents the linear function ε. The crossings with the other lines define the QP energies $\varepsilon_\nu^{\mathrm{QP}}$.

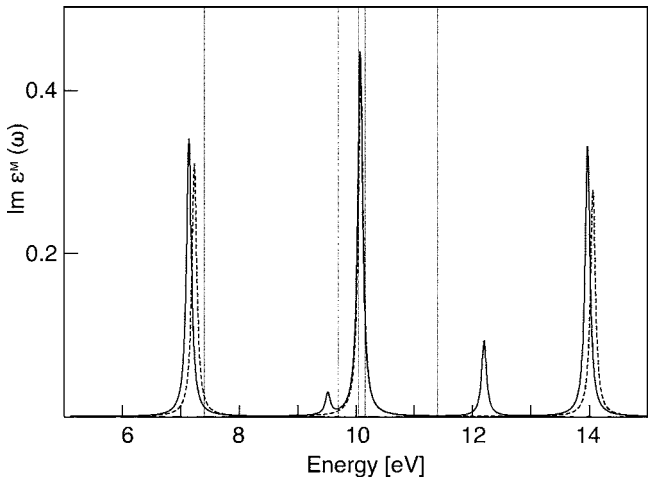

FIG. 16. Optical absorption spectrum of the H_2O molecule including quasiparticle and excitonic effects calculated with six (solid line) and five states (dashed line). Vertical dotted lines indicate the measured singlet pair excitations (cf. data collection in Ref. 92). The optical anisotropy has been neglected and an averaged spectrum is shown.

V. SUMMARY AND CONCLUSIONS

We have shown that the many-body perturbation theory based on Green's functions and an electron self-energy in Hedin's GW approximation can be successfully applied to investigate electronic single-particle and two-particle excitations of molecules. SiH_4, Si_2H_6, and H_2O were studied as prototypical molecules. We have shown that the computed excitation energies are close to the measured values, with maximum deviations smaller than 0.5 eV. The accuracy of the Green's function method is thus similar to that of sophisticated quantum chemistry methods. This is somewhat surprising, given that the approach to treat the electron-electron interaction in the presence of electrons, holes, or electron-hole pair excitations is based on the physical description of a dynamical screening response. However, the treatment of the interaction effects on the same footing, i.e., the GW approximation for the self-energy and the electron-hole attraction,

and the accurate computation of the frequency- and wave-vector-dependent dielectric tensor, obviously ensure excellent results for the energies and the spectral strengths of electronic excitations also for small systems with localized electronic states.

For numerical reasons, but also because of future applications to large systems with both extended and localized electronic states, the considered molecules were modeled in sc supercells. It turns out that the size of the supercell is a very critical issue in several respects. The edge length has to be large enough to avoid coupling of the molecule with its images via electron-electron interaction or related to local-field effects. Numerical criteria of a sufficient supercell size are the vanishing wave-vector dispersion of the bands and the vanishing splittings of states that should be symmetry degenerate. In contrast to true crystals, the continuum of scattering states with energies above the vacuum level is difficult to describe. There may be spurious effects due to an artificial localization of such states in the supercell and related to the number of such states. Fortunately, for not too large excitation energies the effect of the scattering states is surpressed in both the self-energy and optical-spectra calculations when increasing the supercell size. In that case the molecular states below the ionization edge dominate the results. This suggests to restrict the many-body calculation to those molecular states below the vacuum level that are already needed to obtain converged results for the ground state. However, for computing the screening function many more states, occasionally more than one-thousand, have to be used in order to ensure the correct variation of the self-energy for large excitation energies.

Given that molecular single-particle and spin-singlet pair excitations have energies of typically about 10 eV, the relative accuracy of the Bloch function GW/BSE method for molecular studies is comparable to that achieved for bulk crystals with fundamental quasiparticle gaps of about 2 eV and an average error bar of the calculations of roughly 0.1 eV. In the latter case, quasiparticle shifts are of the order of 1 eV, and the redshift of the optical absorption caused by excitonic effects is typically of the order of 0.1 eV. The relative accuracy of the computations for the electronic excitations is the same, irrespective of the localization of the electronic states. The described method is therefore suitable to describe electronic excitations in hybrid systems, containing both extended and localized states. The many-body perturbation theory thus allows for studying, e.g., interfaces formed between crystalline solids and organic or biologically active molecules. Starting from the density functional theory, the calculations can be performed without any experimental parameter.

ACKNOWLEDGMENTS

This work has been supported by the European Community in the framework of the Network of Excellence NANOQUANTA (Contract No. NMP4-ET-2004-500198). Generous grants of supercomputer time from the Höchstleistungsrechenzentrum Stuttgart and the Leibniz-Rechenzentrum München are gratefully acknowledged.

[1] J. T. Yates, Jr., Science **279**, 335 (1998).
[2] C. Joachim, J. K. Ginzewski, and A. Aviram, Nature (London) **408**, 541 (2000).
[3] S. F. Bent, Surf. Sci. **500**, 879 (2002).
[4] M. Preuss, W. G. Schmidt, and F. Bechstedt, Phys. Rev. Lett. **94**, 236102 (2005).
[5] P. Hohenberg and W. Kohn, Phys. Rev. **136**, B864 (1964).
[6] W. Kohn and L. J. Sham, Phys. Rev. **140**, A1133 (1965).
[7] D. M. Ceperley and B. J. Alder, Phys. Rev. Lett. **45**, 566 (1980).
[8] J. P. Perdew and A. Zunger, Phys. Rev. B **23**, 5048 (1981).
[9] J. P. Perdew, in *Electronic Structure of Solids '91*, edited by P. Ziesche and H. Eschrig (Akademie-Verlag, Berlin, 1991).
[10] J. P. Perdew and Y. Wang, Phys. Rev. B **45**, 13244 (1992).
[11] J. P. Perdew, M. Ernzerhof, and K. Burke, J. Chem. Phys. **105**, 9982 (1996).
[12] W. Koch and M. C. Holthausen, *A Chemists' Guide to Density Functional Theory* (Wiley-VCH, Weinheim, 2001).
[13] R. O. Jones and O. Gunnarsson, Rev. Mod. Phys. **61**, 689 (1989).
[14] M. Preuss, W. G. Schmidt, K. Seino, J. Furthmüller, and F. Bechstedt, J. Comput. Chem. **25**, 112 (2004).
[15] H. -Ch. Weissker, J. Furthmüller, and F. Bechstedt, Phys. Rev. B **65**, 155327 (2002).
[16] L. Serrano-Andrés and M. Merchán, J. Mol. Struct.: THEOCHEM **729**, 109 (2005).
[17] J. B. Foresman, M. Head-Gordon, J. A. Pople, and M. J. Frisch, J. Phys. Chem. **96**, 135 (1992).
[18] C. J. Cramer, *Essentials of Computational Chemistry* (Wiley, Chichester, 2002).
[19] T. Helgaker, P. Jørgensen, and J. Olsen, *Estructure - Structure Theory* (Wiley, Chichester, 2000).
[20] E. Runge and E. K. U. Gross, Phys. Rev. Lett. **52**, 997 (1984).
[21] M. E. Casida, in *Recent Developments and Applications of Modern Density Functional Theory*, edited by J. M. Seminario (Elsevier Science B.V., Amsterdam, 1996).
[22] I. Vasiliev, S. Öğut, and J. R. Chelikowsky, Phys. Rev. B **65**, 115416 (2002).
[23] R. E. Stratmann, G. E. Scuseria, and M. J. Frisch, J. Chem. Phys. **109**, 8218 (1998).
[24] J. Oddershede, Adv. Chem. Phys. **69**, 201 (1987).
[25] J. V. Ortiz, Adv. Quantum Chem. **35**, 33 (1999).
[26] L. Hedin, Phys. Rev. **139**, A796 (1965).
[27] L. Hedin and S. Lundqvist, Solid State Phys. **23**, 1 (1969).
[28] G. Onida, L. Reining, and A. Rubio, Rev. Mod. Phys. **74**, 601 (2002).
[29] L. J. Sham and T. M. Rice, Phys. Rev. **144**, 708 (1916).
[30] G. Strinati, Phys. Rev. Lett. **49**, 1519 (1982); Phys. Rev. B **29**, 5718 (1984); Riv. Nuovo Cimento **11**, 1 (1988).
[31] M. S. Hybertsen and S. G. Louie, Phys. Rev. Lett. **55**, 1418 (1985); M. S. Hybertsen and S. G. Louie, Phys. Rev. B **34**, 5390 (1986).

[32] R. W. Godby, M. Schlüter, and L. J. Sham, Phys. Rev. Lett. **56**, 2415 (1986); R. W. Godby, M. Schlüter, and L. J. Sham, Phys. Rev. B **37**, 10159 (1988).
[33] F. Bechstedt, Adv. Solid State Phys. **32**, 161 (1992).
[34] F. Aryasetiawan and O. Gunnarsson, Rep. Prog. Phys. **61**, 237 (1998).
[35] W. G. Aulbur, L. Jönsson, and J. W. Wilkins, Solid State Phys. **54**, 1 (1999).
[36] M. Rohlfing and S. G. Louie, Phys. Rev. B **62**, 4927 (2002).
[37] W. G. Schmidt, S. Glutsch, P. H. Hahn, and F. Bechstedt, Phys. Rev. B **67**, 085307 (2003).
[38] S. Albrecht, L. Reining, R. Del Sole, and G. Onida, Phys. Rev. Lett. **80**, 4510 (1998).
[39] L. X. Benedict, E. L. Shirley, and R. B. Bohn, Phys. Rev. Lett. **80**, 4514 (1998); L. X. Benedict, E. L. Shirley, and R. B. Bohn, Phys. Rev. B **57**, R9385 (1998).
[40] M. Rohlfing and S. G. Louie, Phys. Rev. Lett. **81**, 2312 (1998).
[41] N. -P. Wang, M. Rohlfing, P. Krüger, and J. Pollmann, Phys. Rev. B **67**, 115111 (2003).
[42] P. H. Hahn, W. G. Schmidt, K. Seino, M. Preuss, F. Bechstedt, and J. Bernholc, Phys. Rev. Lett. **94**, 037404 (2005).
[43] M. Rohlfing and S. G. Louie, Phys. Rev. Lett. **83**, 856 (1999).
[44] P. H. Hahn, W. G. Schmidt, and F. Bechstedt, Phys. Rev. Lett. **88**, 016402 (2002).
[45] E. K. Chang, E. L. Shirley, and Z. H. Levine, Phys. Rev. B **65**, 035205 (2002).
[46] R. Leitsmann, W. G. Schmidt, P. H. Hahn, and F. Bechstedt, Phys. Rev. B **71**, 195209 (2005).
[47] A. Hermann, W. G. Schmidt, and F. Bechstedt, Phys. Rev. B **71**, 153311 (2005); A. Hermann, W. G. Schmidt, and F. Bechstedt, J. Phys. Chem. B **109**, 7928 (2005).
[48] J. Furthmüller, G. Cappellini, H. -Ch. Weissker, and F. Bechstedt, Phys. Rev. B **66**, 045110 (2002).
[49] F. Sottile, V. Olevano, and L. Reining, Phys. Rev. Lett. **91**, 056402 (2003).
[50] A. Marini, R. Del Sole, and A. Rubio, Phys. Rev. Lett. **91**, 256402 (2003).
[51] G. Adragna, R. Del Sole, and A. Marini, Phys. Rev. B **68**, 165108 (2003).
[52] M. E. Casida and D. P. Chong, Phys. Rev. A **40**, 4837 (1989).
[53] E. L. Shirley and R. M. Martin, Phys. Rev. B **47**, 15404 (1993); **47**, 15413 (1993).
[54] G. Onida, L. Reining, R. W. Godby, R. Del Sole, and W. Andreoni, Phys. Rev. Lett. **75**, 818 (1995).
[55] M. Rohlfing and S. G. Louie, Phys. Rev. Lett. **80**, 3320 (1998); **82**, 1959 (1999).
[56] L. Reining, O. Pulci, M. Palummo, and G. Onida, Int. J. Quantum Chem. **77**, 951 (2000).
[57] M. Rohlfing, Int. J. Quantum Chem. **80**, 807 (2000).
[58] Y. Ohta, J. Maki, T. Yoshimoto, Y. Shigeta, H. Nagao, and K. Nishikawa, Int. J. Quantum Chem. **84**, 348 (2001).
[59] Y. Shigeta, A. M. Ferreira, V. G. Zakrzewski, and J. V. Ortiz, Int. J. Quantum Chem. **85**, 411 (2001).
[60] D. R. Hamann, Phys. Rev. B **40**, 2980 (1989).
[61] E. L. Briggs, D. J. Sullivan, and J. Bernholc, Phys. Rev. B **54**, 14362 (1996).
[62] N. Troullier and J. L. Martins, Phys. Rev. B **43**, 1993 (1991).
[63] G. Kresse and D. Joubert, Phys. Rev. B **59**, 1758 (1999).
[64] G. Kresse and J. Furthmüller, Phys. Rev. B **54**, 11169 (1996); Comput. Mater. Sci. **6**, 15 (1996).
[65] B. Adolph, J. Furthmüller, and F. Bechstedt, Phys. Rev. B **63**, 125108 (2001).
[66] G. D. Mahan, *Many-Particle Physics* (Plenum Press, New York, 1990).
[67] F. Bechstedt, M. Fiedler, C. Kress, and R. Del Sole, Phys. Rev. B **49**, 7357 (1994).
[68] A. Fleszar and W. Hanke, Phys. Rev. B **56**, 10228 (1997).
[69] C. Blomberg and B. Bergersen, Can. J. Phys. **50**, 2286 (1972).
[70] B. Bergersen, F. W. Kus, and C. Blomberg, Can. J. Phys. **51**, 102 (1973).
[71] S. L. Adler, Phys. Rev. **126**, 413 (1962).
[72] N. Wiser, Phys. Rev. **129**, 62 (1963).
[73] R. Del Sole and E. Fiorino, Phys. Rev. B **29**, 4631 (1984).
[74] W. Hanke and L. J. Sham, Phys. Rev. Lett. **43**, 387 (1979); Phys. Rev. B **21**, 4656 (1980).
[75] F. Bechstedt, K. Tenelsen, B. Adolph, and R. Del Sole, Phys. Rev. Lett. **78**, 1528 (1997).
[76] S. Glutsch, D. S. Chemla, and F. Bechstedt, Phys. Rev. B **54**, 11592 (1996).
[77] G. Onida and W. Andreoni, J. Chem. Phys. **243**, 183 (1995).
[78] J. C. Grossman, M. Rohlfing, L. Mitas, S. G. Louie, and M. L. Cohen, Phys. Rev. Lett. **86**, 472 (2001).
[79] I. Vasiliev and R. M. Martin, Phys. Rev. A **69**, 052508 (2004).
[80] R. van Leeuwen and E. J. Baerends, Phys. Rev. A **49**, 2421 (1994).
[81] M. E. Casida and D. R. Salahub, J. Chem. Phys. **113**, 8918 (2000).
[82] U. Itoh, Y. Toyoshima, and H. Onuki, J. Chem. Phys. **85**, 4867 (1986).
[83] A calculation done with the VASP code and an automatic symmetrization yields KS orbitals similar to the QP ones shown in Fig. 6.
[84] I. Vasiliev, S. Ögüt, and J. Chelikowsky, Mater. Res. Soc. Symp. Proc. **579**, 91 (2000).
[85] L. X. Benedict, A. Puzder, A. J. Williamson, J. C. Grossman, G. Galli, J. E. Klepeis, J. -Y. Raty, and O. Pankratov, Phys. Rev. B **68**, 085310 (2003).
[86] I. Vasiliev, Phys. Status Solidi B **239**, 19 (2003).
[87] W. S. Benedict, N. Gailan, and E. K. Plyler, J. Chem. Phys. **24**, 1139 (1956).
[88] X. Xu and W. A. Goddard, J. Phys. Chem. A **108**, 2305 (2004).
[89] C. -H. Hu and D. P. Chong, J. Chin. Chem. Soc. (Taipei) **47**, 141 (2000).
[90] C. R. Brundle and D. W. Turner, Proc. R. Soc. London, Ser. A **307**, 27 (1968).
[91] K. Kimura, S. Katsumata, Y. Achiba, T. Yamazaki, and S. Iwata, *Handbook of HeI Photoelectron Spectra of Fundamental Organic Molecules* (Halsted, New York, 1981).
[92] B. D. Bursulaya, J. Jeon, D. A. Zichi, and H. J. Kim, J. Chem. Phys. **108**, 3286 (1998).
[93] D. M. Chipman, J. Chem. Phys. **122**, 044111 (2005).
[94] Z. -L. Cai, D. J. Tozer, and J. R. Reimers, J. Chem. Phys. **113**, 7084 (2000).